Oxygenated products formed from OH-initiated reactions of trimethylbenzene: Autoxidation and accretion

Yuwei Wang[1], Archit Mehra[2], Jordan E. Krechmer[3], Gan Yang[1], Xiaoyu Hu[1], Yiqun Lu[1], Andrew Lambe[3], Manjula Canagaratna[3], Jianmin Chen[1], Douglas Worsnop[3], Hugh Coe[2], Lin Wang[1,4,5] *

[1] Shanghai Key Laboratory of Atmospheric Particle Pollution and Prevention (LAP[3]), Department of Environmental Science and Engineering, Jiangwan Campus, Fudan University, Shanghai 200438, China
[2] Centre for Atmospheric Science, School of Earth and Environment Sciences, The University of Manchester, Manchester, M13 9PL, UK
[3] Center for Aerosol and Cloud Chemistry, Aerodyne Research Inc., Billerica, MA, USA
[4] Collaborative Innovation Center of Climate Change, Nanjing 210023, China
[5] Shanghai Institute of Pollution Control and Ecological Security, Shanghai 200092, China

** Corresponding Author: L.W., email, lin_wang@fudan.edu.cn; phone, +86-21-31243568*

Abstract. Gas-phase oxidation pathways and products of anthropogenic volatile organic compounds (VOCs), mainly aromatics, are the subject of intensive research with attention paid to their contributions to secondary organic aerosol (SOA) formation and potentially, new particle formation (NPF) in the urban atmosphere. In this study, a series of OH-initiated oxidation experiments of trimethylbenzene (TMB, C_9H_{12}) including 1,2,4-TMB, 1,3,5-TMB, 1,2,3-TMB, and 1,2,4-(methyl-D3)-TMBs ($C_9H_9D_3$) were investigated in an oxidation flow reactor (OFR), in the absence and presence of NO_x. Products were measured using a suite of state-of-the-art instruments, i.e., a nitrate-based chemical ionization - atmospheric pressure interface time-of-flight mass spectrometer (Nitrate CI-APi-TOF), an iodide-adduct chemical ionization - time-of-flight mass spectrometer (Iodide CI-TOF) equipped with a Filter Inlet for Gases and AEROsols (FIGAERO), and a Vocus proton-transfer-reaction mass spectrometer (Vocus PTR). A large number of C9 products with 1-11 oxygen atoms and C18 products presumably formed from dimerization of C9 peroxy radicals were observed, hinting the extensive existence of autoxidation and accretion reaction pathways in the OH-initiated oxidation reactions of TMBs. Oxidation products of 1,2,4-(methyl-D3)-TMBs with deuterium atoms in different methyl substituents were then used as a molecular basis to propose potential autoxidation reaction pathways. Accretion of C9 peroxy radicals is the most significant for aromatics with meta-substituents and the least for aromatics with ortho-substituents, if the number and size of substituted groups are identical. The presence of NO_x would suppress the formation of C18 highly oxygenated molecules (HOMs) and enhance the formation of organonitrates, and even dinitrate organic compounds. Our results show that the oxidation products of TMB are much more diverse and could be more oxygenated than the current mechanisms predict.

1 Introduction

Oxidation products of volatile organic compounds (VOCs) contribute significantly to the formation of secondary organic aerosols (SOAs) (Ng et al., 2010; Zhang et al., 2007), which raises a globally ubiquitous health and environmental concern (Hallquist et al., 2009). There have been numerous studies that aim to construct detailed VOC oxidation mechanisms to advance our understanding on VOC degradation, SOA formation, and ozone formation (Atkinson, 1986; Atkinson and Arey, 2003; Atkinson and Carter, 1984; Kroll and Seinfeld, 2008; Ziemann and Atkinson, 2012). Based on the hypothesis that the products and

kinetics of many unstudied chemical reactions can be proposed by analogy to known reactions of similar chemical species (Ziemann and Atkinson, 2012) and/or predicted by the structure-activity relationships (Kwok and Atkinson, 1995), the Master Chemical Mechanism (MCM) is developed as a nearly explicit chemical mechanism, describing the degradation of numerous VOCs (Bloss et al., 2005; Jenkin et al., 2003; Saunders et al., 2003). Due to the high complexity of VOC oxidation processes, it is not surprising that mechanisms leading to the formation of previously unidentified species are still missing.

The formation of highly oxygenated organic molecules (HOMs) through the autoxidation pathway during VOC oxidation is such an example. HOMs refer to organic compounds typically containing six or more oxygen atoms that are formed in the gas phase (Bianchi et al., 2019). Autoxidation is a chemical process where an alkyl peroxy radical (RO_2) undergoes an intramolecular hydrogen shift followed by addition of a molecular oxygen, resulting in a more oxygenated RO_2 radical (Crounse et al., 2013; Ehn et al., 2014). It is an effectively repetitive uni-molecular reaction as the more oxidized RO_2 will serve as a parent RO_2 in the next autoxidation reaction, leading to the rapid formation of HOMs in very short time scales (Bianchi et al., 2019; Jørgensen et al., 2016).

Owing to recent developments in the analytical techniques such as nitrate-anion chemical ionization mass spectrometry (nitrate CIMS), our knowledge on the autoxidation pathway during the oxidation of biogenic volatile organic compounds (BVOCs) has been significantly improved. Certain systems, such as the oxidation of monoterpenes, have been studied extensively, of which ozonolysis has been confirmed as an important source for HOMs (Ehn et al., 2014; Jokinen et al., 2014). The OH-initiated oxidation is also a considerable HOM formation source for monoterpenes and isoprene (Krechmer et al., 2015), albeit at lower yields for monoterpenes containing an endocyclic double bond (Jokinen et al., 2014, 2015; Rissanen et al., 2015). Detailed mechanisms of monoterpene-derived HOM formation reactions, initiated by ozone or OH, were investigated through theoretical calculations (Berndt et al., 2016), or by analogy to reactions of similar chemical species, i.e., cyclohexene (Rissanen et al., 2014). A couple of studies performed H/D isotope exchange experiments, which can probe the number of hydrogen atoms other than that in C-H, strongly supporting the proposal of autoxidation mechanisms (Ehn et al., 2014; Rissanen et al., 2014). Research on other BVOCs, i.e., isoprene and sesquiterpenes (Crounse et al., 2013; Richters et al., 2016; Teng et al., 2017), and on other oxidants, i.e., NO_3 and chlorine (Nah et al., 2016; Wang et al., 2020), indicate the widespread existence of autoxidation pathways in the oxidation of BVOCs. The products formed from autoxidation of biogenic precursors have been proven to play a vital role in atmospheric new particle formation (NPF) because of their low volatility (Ehn et al., 2014; Stolzenburg et al., 2018; Tröstl et al., 2016).

On the other hand, studies on autoxidation of anthropogenic VOCs are rather sparse. Wang et al. (2017) theoretically and experimentally showed the autoxidation route of alkylbenzenes to form HOMs in the gas phase. Identities and yields of HOM products from different aromatics were systematically measured and the determined molar HOM yields were in the range of 0.1 % to 2.5 %, which are similar to the molar HOM yields of OH-initiated reactions of BVOCs (Jokinen et al., 2015; Molteni et al., 2018). Currently, aromatics-derived HOMs are believed to be formed via many reaction pathways, including accretion, bicyclic intermediate reactions, and multi-generation OH reactions (Berndt et al., 2018b; Garmash et al., 2020; Zaytsev et al., 2019). The unimolecular isomerization and autoxidation reactions of aromatic peroxy

radicals have been shown to be fast enough to compete with other bimolecular reactions even under NO concentrations as high as in urban environment (Tsiligiannis et al., 2019).

Trimethylbenzene (TMB) including isomers of 1,3,5-TMB, 1,2,3-TMB, and 1,2,4-TMB is one of the most common anthropogenic VOCs in urban areas. OH-initiated oxidation of TMB is its dominant chemical loss in the atmosphere (Atkinson and Arey, 2003), which proceeds either via H atom abstraction from the methyl substituents or via addition of OH radical onto the aromatic ring (Ziemann and Atkinson, 2012). The H atom abstraction channel is minor in the OH-induced oxidation reactions of TMB, forming dimethyl-benzaldehyde. The major channels of OH addition consist of peroxide-bicyclic pathway, phenolic pathway, and epoxy-oxy pathway (Bloss et al., 2005; Calvert et al., 2002; Jenkin et al., 2003). The three TMB isomers have different branching ratios for these pathways resulting from the substitution-, site-, and stereo-specificity, however specific branching ratios are still in debate. Among these pathways, the peroxide-bicyclic pathway has the highest branching ratio and can form bicyclic peroxy radicals (BPRs), which are important intermediates that contribute significantly to the formation of HOMs (Wang et al., 2017). Subsequent reactions of the intermediates will lead to the formation of stabilized products (or non-radical products). On the other hand, the details of the autoxidation mechanisms for anthropogenic precursors remain elusive. Direct measurements of individual H-shift rates, the detailed structure of HOMs, and a robust quantification of HOM yields are still lacking. The detailed kinetics for termination reactions of different RO_2 are also ambiguous. Consequently, it is hard to comprehensively judge the TMB oxidation reaction pathways and products under different atmospheric conditions, and to evaluate the contribution of TMB oxidation to atmospheric NPF and SOA formation.

In this study, we studied the OH-initiated oxidation of 1,3,5-TMB, 1,2,3-TMB, and 1,2,4-TMB with a focus on autoxidation and accretion products, via the concurrent usage of a Vocus proton-transfer-reaction time-of-flight mass spectrometry (Vocus PTR), an iodide-adduct chemical ionization - time-of-flight mass spectrometer equipped with a Filter Inlet for Gases and AEROsols (FIGAERO Iodide CI-TOF), and a nitrate-based chemical ionization - atmospheric pressure interface time-of-flight mass spectrometer (Nitrate CI-APi-TOF). Oxidation of 1,2,4-(methyl-D3)-TMBs was investigated to elucidate the detailed autoxidation reaction pathway. The influence of NO_x concentration on product distribution was also investigated.

2 Methods

As shown in Figure 1, oxidation experiments of TMB were conducted in a Potential Aerosol Mass (PAM) oxidation flow reactor (OFR, Aerodyne Research, Inc.). A self-prepared VOC cylinder was used to provide a constant source of gaseous TMB as a reactant. O_3/OH was produced in-situ in the PAM and the relative humidity (RH) was regulated by the PAM setup, which will be introduced in details later. A Vocus PTR (Krechmer et al., 2018), a FIGEARO Iodide CI-TOF (Lee et al., 2014; Lopez-Hilfiker et al., 2014), and a Nitrate CI-APi-TOF (Ehn et al., 2014; Eisele and Tanner, 1993) were deployed to detect gaseous products as well as particulate ones. In addition, an ozone monitor (Model 106-M, 2B technologies) was utilized to measure ozone concentration, whereas a set of Scanning Mobility Particle Sizer (SMPS, consisting of one TSI Model 3080 Long DMA and one TSI Model 3776 Condensation Particle Counter) was employed to measure the number size distribution of submicron aerosol particles.

OFR. In this study, the sum of all the flows in the PAM, including a zero air flow, an ozone (O_3) flow, a TMB/N_2 flow, and a N_2O/N_2 flow depending upon experimental conditions, was kept at either 10 or 10.4 slpm (standard litres per minute, standard to 0 ℃, 1 atm), resulting in calculated mean residence times of approximately 80 seconds (77.3 seconds at 10.4 slpm). Zero air was generated by a zero gas generator (Sabio Model 1001 Zero Gas Source). A fraction of the zero air was passed through a Nafion humidifier (Perma Pure Model FC100-80-6MSS) filled with ultrapure water to achieve the desired RH in the OFR. Ozone was generated by passing 800 sccm (standard cubic centimetre, standard to 0 ℃, 1 atm) of zero air through a separate ozone chamber and input into the OFR. In order to create a low HO_2/RO_2 ratio environment to promote the carbonyl and hydroxyl channels to terminate RO_2 radicals, the OFR was operated with only the 254 nm lights on (Lambe et al., 2019), which is referred to as OFR254 mode in previous studies (Peng et al., 2015). In OFR254 mode, the primary oxidant production reactions in the OFR are:

$$O_3 + hv(254\,nm) \rightarrow O_2 + O(^1D) \qquad (R1)$$

$$O(^1D) + H_2O \rightarrow 2OH \qquad (R2)$$

In some experiments, N_2O (99.999%, Air Liquide) was added at the OFR inlet, corresponding to mixing ratios of 3.4% of the total gas flow rates, which produced NO_x via the following reactions (Lambe et al., 2017):

$$N_2O + O(^1D) \rightarrow 2NO \qquad (R3)$$

$$NO + O_3 \rightarrow NO_2 + O_2 \qquad (R4)$$

A photochemical model (PAM_chem_v8) (Lambe et al., 2017; Li et al., 2015; Peng et al., 2015) was implemented to constrain the NO/NO_2 profiles in the experiments, whose details are presented in Section S1.

Before each experiment, the PAM OFR was purged with zero air under the OFR254 operation mode until the signals of acetic acid and other common VOC oxidation products decreased to background levels of the Vocus PTR and CI-TOF that are described below.

Vocus PTR. The newly developed Vocus PTR has a high sensitivity to a wide range of VOCs and oxygenated volatile organic compounds (OVOCs) (Krechmer et al., 2018; Li et al., 2019; Riva et al., 2019). Its mass resolving power (m/Δm = ~12000 at 200 Th, 1 Th = 1 *u/e*, where *e* is the elementary charge and *u* is the atomic mass unit) allows to simultaneously monitor many isobaric species, and even to distinguish the very minor mass discrepancy (0.001548 *u*) between one deuterium atom and two hydrogen atoms. The instrument background together with a quantitative calibration by injection of standards was measured between every two experiments to minimize potential inaccuracies. In our study, the pressure of the focusing ion-molecule reactor (FIMR) was actively maintained at 1.5 mbar resulting in an E/N of the FIMR at 110 Td (1 Td = 1×10^{-17} V cm^2), which was generally a moderate operating condition leading to relatively little fragmentation of compounds of interest (Gueneron et al., 2015; Yuan et al., 2017).

FIGAERO-Iodide CI-TOF. The Iodide-adduct CI-TOF is able to determine elemental compositions of a suite of atmospheric oxygenated organic species (D'Ambro et al., 2017; Lee et al., 2014; Lopez-Hilfiker et al., 2016). It has increasing sensitivities toward more polar and acidic VOCs (Lee et al., 2014). The mass resolution of the Iodide CI-TOF was tuned to be around 3000. The reagent ion (I^-) was produced from permeated CH_3I vapor in N_2 by a radioactive source of Am-241 (0.1 mCi). The pressure in the ion-molecule

reactor (IMR) was regulated at 100 mbar, whereas the small segmented quadrupole (SSQ) pressure was set to be around 2 mbar. The FIGAERO inlet manifold enables the Iodide CI-TOF to measure both gas and particle compositions at a molecular level (Lopez-Hilfiker et al., 2014). In our study, aerosols were collected onto a PTFE filter (5μm, Millipore) at 0.96 slpm for 20 min, while the gases were measured simultaneously via a separate dedicated port. Then, a thermal desorption cycle was started 2 minutes after the FIGAERO filter was aligned to a heating tube, through which a heated ultra-high purity nitrogen flow was passed and heated according to a pre-programmed temperature ramp. The ultra-high purity nitrogen was initially held at 25 ℃ for 2 min, and then heated at a rate of 10 ℃ min^{-1} to 200 ℃, which was maintained for the remainder of the temperature ramp (50 min in total).

Nitrate CI-APi-TOF. The Nitrate CI-APi-TOF has been increasingly used for the measurement of low volatility organic compounds (LVOC) and extremely low volatility organic compounds (ELVOCs) (Ehn et al., 2014; Hyttinen et al., 2015; Jokinen et al., 2014), which mostly have a high O:C ratio. The resolving power of the Nitrate CI-APi-TOF was up to around 8000 in our study. The selectivity of nitrate ions keeps the spectrum clean from the more abundant, less oxidized compounds in our experiments. Most of the detected species were observed exclusively as adducts with NO_3^-, a very minor fraction of which contain odd hydrogen numbers and are hence postulated to be radicals but not presented in this manuscript.

The concurrent use of three mass spectrometers (MSs) with different reagent ions allows us to obtain a comprehensive picture of the oxidation products of TMB with OH radicals. The detection suitability of these three instruments for oxidation products with various levels of oxidation has been discussed a lot in previous studies (Isaacman-VanWertz et al., 2017; Krechmer et al., 2018; Riva et al., 2019). Generally, Vocus PTR displays selectivity for less oxidized compounds; Iodide CI-TOF favors more oxygenated species; and Nitrate CI-APi-TOF shows the highest efficiency for the most oxidized compounds. Dimer products of TMB oxidation are expected to be detected by Nitrate CI-APi-TOF as clusters with NO_3^-, which is due to the potential hydrogen bond donor functional groups in these molecules, inferred from the abundant oxygen and hydrogen atoms in the formulas. These products should not be detected by Vocus PTR. One explanation is that these molecules are likely to be fragile and therefore have fragmented owing to the protonation or the strong electric field in the FIMR of Vocus PTR. Alternatively, these products might not go through the PEEK tube inlet of Vocus PTR. At the same time, the sample inlet for Iodide CI-TOF in our experiments is not desirable for the detection of dimer products.

To ensure that the reported signal is truly from the sample flow instead of internal background or contamination, subtraction of the mass spectra for the OFR background from the samples has been performed for each instrument. In addition, since this study is mostly concerned with identification of oxidation products from OH-initiated reactions of TMBs and elucidation of the potential autoxidation pathway, Nitrate CI-APi-TOF and Iodide CI-TOF were hence not calibrated and only the arbitrary signals with MS transmission correction (Heinritzi et al., 2016; Krechmer et al., 2018) were compared within the same instrument. It should then be noted that the relative signal intensities are biased among the MSs because of their ionization methods and transmission efficiency.

In each experiment, the Vocus PTR was used to confirm the establishment of stable precursor gas concentrations, and then the pair of 254 nm Hg lamps were turned on to generate the OH radicals and reaction products were analyzed by the MSs. The input RH in the OFR was kept at a low level and the voltage of the Hg lamps was slightly tuned in every experiment, so that the OH exposure in the OFR was

close to one oxidation lifetime of TMB, i.e., consumption of (1-1/*e*) of the initial TMB. Under this condition, the production of the first-generation products is generally favoured and the multi-generation products are also present, if the subsequent loss reactions for these products are assumed to proceed in the similar rate.

Table 1 summarizes all the experiments that were performed. Studied were 1,3,5-TMB (≥ 99.0%, Aladdin), 1,2,3-TMB (Analytical standard, Aladdin), 1,2,4-TMB (≥ 99.5%, Aladdin), 1,2,4-(1-methyl-D3)-TMB (≥ 95%, Qingdao Tenglong Weibo Technology Co., Ltd., China), 1,2,4-(2-methyl-D3)-TMB (≥ 95%, Qingdao Tenglong Weibo Technology Co., Ltd., China), and 1,2,4-(4-methyl-D3)-TMB (≥ 95%, Qingdao Tenglong Weibo Technology Co., Ltd., China). The structure of these partially deuterated TMBs can be found in Figure S1. Note that ozone reactions were not taken into account in this study, because ozone reacts with aromatics at negligible rates, and its reaction rate with oxidation products containing C=C double bonds is much slower compared with that of OH (Jenkin et al., 1997, 2003; Molteni et al., 2018; Saunders et al., 2003). Also note that the concentrations of precursors in our experiments were much higher than the atmospheric ones. These concentrations were deliberately chosen to help identify the highly oxygenated products that are of low volatility and easy to loss in the sampling, but subject to the side effect that the relative significance of different pathways could be altered.

3 Results and discussion

3.1 Characteristics of C9 products

Figure 2 presents an overview of C7, C8 and C9 products in a carbon oxidation state ($\overline{OS}_C$)-carbon number (n_C) space as observed by three MSs and also those predicted by MCM v3.3.1. Carbon oxidation state is a quantity that increases with the level of oxidation, which reveals the chemical aging of atmospheric organics (Kroll et al., 2011). It is evident that more species were detected by the three MSs, and although there were clear differences between products detected from different MSs, results indicate missing oxidation pathways in the current versions of the MCM (MCM v3.3.1, available at: http://mcm.leeds.ac.uk/MCM). Oxygen-containing C9 products were formed by adding functional groups to the carbon skeleton, whereas C7 and C8 products resulted from carbon-carbon scission of the original carbon skeleton together with functionalization. A large proportion of C7-C9 products were more oxidized than those predicted by MCM, hinting the existence of highly efficient oxidation pathways.

Recent studies have emphasized on the importance of the peroxide-bicyclic pathway in producing highly oxygenated compounds in the oxidation of alkylbenzenes (Wang et al., 2017; Zaytsev et al., 2019), which leads to the formation of ring-retaining products. Therefore, here we further investigated C9 products of TMB oxidation detected by the three MSs (Figure 3). $C_9H_{10}O_{1\text{-}6}$, $C_9H_{12}O_{1\text{-}7}$, and $C_9H_{14}O_{4\text{-}6}$ contributed to the most of the signal intensities in Vocus PTR (Figure 3a). Compounds with fewer hydrogen atoms than TMB in Vocus PTR might be formed from hydrogen abstraction reactions. Iodide CI-TOF detected products with five to seven oxygen atoms (Figures 3b & 3c), which is narrower compared with Vocus PTR and Nitrate CI-APi-TOF. Molecules with 18 hydrogen atoms were detected only in Iodide CI-TOF, which is an unexpected high number. These molecules, low in signal intensities in both gas and particle phases, might be formed from multiple OH attacks since each OH attack can only add two hydrogens in maximum onto the parent molecule. The species with the highest signal intensities measured in the gas phase appeared to be $C_9H_{12}O_4$, $C_9H_{12}O_6$, $C_9H_{14}O_5$, and $C_9H_{14}O_6$ in the 1,2,4-TMB + OH experiment, $C_9H_{14}O_5$ and $C_9H_{14}O_6$

in the 1,3,5-TMB + OH experiment, and $C_9H_{12}O_6$ and $C_9H_{12}O_7$ in the 1,2,3-TMB + OH experiment (Figure 3b). Compared with the gas phase, more oxidized particulate products tended to contribute a larger proportion of signal in FIGAERO-Iodide-CI-APi-TOF (Figure 3c). Nevertheless, the gas phase products are emphasized in the current study, which can be detected by and compared among the three instruments. Nitrate CI-APi-TOF detected C9 products containing 12-16 hydrogen atoms and 5-11 oxygen atoms (Figure 3d).

RO_2 radicals can react in the absence of NO, to form termination products including carbonyls, alcohols, and hydroperoxides via the following reactions (Mentel et al., 2015).

$$RO_2 + R'O_2 \rightarrow R_HC = O + R' - OH + O_2 \quad (R5)$$

$$RO_2 + R'O_2 \rightarrow ROH + R'_HC = O + O_2 \quad (R6)$$

$$RO_2 + HO_2 \rightarrow ROOH + O_2 \quad (R7)$$

Here we present a criteria method based on the work of Mentel et al. (2015). For a parent peroxy radical with a molecular mass of *m*, its termination ought to lead to the formation of a carbonyl, an alcohol, and a hydroperoxyl, which have a molecular mass of *m*-17, *m*-15, and *m*+1, respectively. Since elemental formulas as determined by the high-resolution MS do not contain information regarding functional groups or the structure of a molecule, the identified mass spectral signals could be counted as either one of the three categories. Listed in Table 2 are detected stabilized oxidation products in categories of carbonyl, alcohol, and hydroperoxyl, which hints the potential existence of the corresponding peroxy radicals. These stabilized products all contain six or more oxygen atoms, which meet the definition of HOMs (Bianchi et al., 2019). $C_9H_{12}O_6$ is one of the only two signals that have been predicted by MCM, assumed to be a hydroperoxyl product from a ring-opening peroxy radical that goes through multiple OH attack reactions (MCM name: C7MOCOCO3H), which is unlikely to contribute a lot to the observed signal of $C_9H_{12}O_6$ since the concentration of a multi-generation product is not expected to be high at OH exposure as short as one lifetime of TMB. $C_9H_{14}O_6$ is the other one, presumed to be a hydroperoxyl product of a second-generation peroxy radical formed via epoxy-oxy pathway (MCM name: TM124MUOOH), which is unlikely to be formed through the MCM route with a considerable yield, either. Four pairs of peroxy radicals, i.e., $C_9H_{13}O_7$· and $C_9H_{13}O_9$•, $C_9H_{13}O_8$• and $C_9H_{13}O_{10}$•, $C_9H_{15}O_7$• and $C_9H_{15}O_9$•, and $C_9H_{15}O_8$• and $C_9H_{15}O_{10}$•, can be selected from the eight potential peroxy radicals in Table 2. The molecular formulas for the peroxy radicals within each pair differ by 2 × O, which is a first evidence for the autoxidation pathway.

3.2 Autoxidation mechanisms of 1,2,4-TMB

The autoxidation pathways were then further elucidated by experiments with isotopically labelled precursors, 1,2,4-(1-methyl-D3)-TMB, 1,2,4-(2-methyl-D3)-TMB, and 1,2,4-(4-methyl-D3)-TMB, whose structure is shown in Figure S1.

If an intramolecular hydrogen shift happens during autoxidation with the abstracted hydrogen coming from a methyl group, molecular oxygen will rapidly attach to this carbon-centred radical to form a new alkyl peroxy radical (Bianchi et al., 2019 and reference herein). One potential fate of this R-CH_2OO• radical is to lose one of the two remaining hydrogen atoms, forming a carbonyl according to Reaction R5. Thus, one of the three original hydrogen atoms in the methyl group will leave this molecule after an autoxidation step (Ehn et al., 2014; Mentel et al., 2015; Molteni et al., 2018; Otkjær et al., 2018; Rissanen et al., 2014;

Wang et al., 2017). In the case of a deuterium abstraction from a methyl-D3 group during the autoxidation, an oxidation product with two deuterium atoms ($C_xH_yD_2O_z$) will then be formed, which is presumably a carbonyl. Although an alcohol or a hydroperoxyl could also be formed from a peroxy radical, it is not suitable to utilize the presence of alcohol and hydroperoxyl products as a criteria to judge the existence of autoxidation. The hydroxyl channel of deuterated peroxy radicals can lead to the formation of alcohol products with either 3 or 4 deuterium atoms, depending on the nature of the other reacting RO_2. The slow unimolecular reaction rate of deuterated methyl group corresponds to little formation of the products with 4 deuterium atoms, whereas our MSs cannot differentiate 3 deuterium atoms either from a molecule with autoxidation and hydroxyl termination or from an untouched methyl-D3 group. On the other hand, the hydroperoxyl channel would lead to the formation of hydroperoxyl products with 3 deuterium atoms, too. Therefore, only the carbonyl channel products of a peroxy radical was used to suggest the potential autoxidation that has occurred.

Table 3 summarizes two-deuterium-containing C9 ($C_9H_yD_2O_z$) products that were detected by Vocus PTR and Nitrate CI-APi-TOF in different isotope labelling experiments: $C_9H_{10}D_2O_6$ in the 1,2,4-(1-methyl-D3)-TMB + OH experiment by Vocus PTR and Nitrate CI-APi-TOF; $C_9H_{10}D_2O_7$ in the 1,2,4-(1-methyl-D3)-TMB + OH experiment by Vocus PTR; and $C_9H_{12}D_2O_8$ in the 1,2,4-(4-methyl-D3)-TMB + OH experiment by Nitrate CI-APi-TOF. $C_9H_{10}O_7D_2$ (234.0703 Th) was expected to be detected by Nitrate CI-APi-TOF, but unfortunately an undefined peak (located at 295.9827 Th) covered the position where $C_9H_{10}O_7D_2{\cdot}NO_3^-$ (296.0592 Th) was supposed to been identified. $C_9H_{12}D_2O_8$ (252.0814 Th) was not detected by Vocus PTR, likely owing to either its low proton affinity or its partitioning onto the inlet of Vocus PTR , given its high O:C ratio and hence low volatility. However, Nitrate CI-APi-TOF was able to detect this very sticky compound, because the nitrate source is constructed with concentric sample and sheath flows that minimize the diffusive losses of samples to the source wall. These results indicate that an intramolecular deuterium-migration happened on the 1-methyl-D3 substituent of the $C_9H_{10}D_3O_4$ and $C_9H_{10}D_3O_5$ radicals, and the 4-methyl-D3 substituent of the $C_9H_{12}D_3O_7$ radical, respectively, then one oxygen was added to the resulting alkyl radicals, and the new peroxy radical reacted to form $C_9H_{10}D_2O_6$, $C_9H_{10}D_2O_7$, and $C_9H_{12}D_2O_9$, respectively.

These three compounds ($C_9H_{10}D_2O_6$, $C_9H_{10}D_2O_7$, and $C_9H_{12}D_2O_9$) did not possess high signal intensities, because the deuterium transfer reactions are typically significantly slower for D (^{2}H) nuclei than hydrogen transfer reactions for H (^{1}H) (Bianchi et al., 2019; Wang et al., 2017). There might be other two-deuterium-containing C9 products in these experiments. However, since many of these signals were at the instrument detection limits or even lower, the nonideal experimental conditions prevent us from confirming more such compounds.

Based on the observed signals of two-deuterium-containing C9 products and structures that have been previously proven to favor H-shift reactions (Otkjær et al., 2018), two plausible formation pathways for the observed products are proposed.

The first one starts with a BPR of $C_9H_{13}O_5{\cdot}$ as shown in Scheme 1, which is the first BPR formed from C_9H_{12} via the peroxide-bicyclic pathway. The structure of this particular $C_9H_{13}O_5{\cdot}$ is different from what is proposed in MCM v3.3.1, but the position for the initial OH attack, i.e., the 4th carbon on the ring, is feasible owing to the attraction of a substituted group on its para-position (Li and Wang, 2014), and the subsequent addition of O_2 after the initial OH attack along with bicyclization occurs on the same relative position as

previous studies have suggested (Bloss et al., 2005; Jenkin et al., 2003). The resulting BPR of $C_9H_{13}O_5$· undergoes a hydrogen shift, during which the abstracted hydrogen comes from the methyl terminal of an allylic group. This hydrogen is much easier to be abstracted, compared to those in a normal methyl group that are unlikely to go through a hydrogen shift with a peroxy radical (Otkjær et al., 2018). The new BPR of $C_9H_{13}O_7$· then reacts via R5, R6, and R7 to form $C_9H_{12}O_6$, $C_9H_{14}O_6$, and $C_9H_{14}O_7$, respectively. This pathway is suggested by the observation of $C_9H_{10}D_2O_6$ in the 1,2,4-(1-methyl-D3)-TMB + OH experiment.

It's noted that in all the three isotope experiments, we also detected products of $C_9H_9D_3O_6$ and $C_9H_9D_3O_7$ with much higher signal intensities, indicating the existence of other autoxidation pathways. Thus, it deserves a repeated emphasis here that we only point out feasible pathways that are supported by our isotope experiments in this work, but do not rule out other possibilities.

The second pathway is described in scheme 2. This pathway starts from a BPR of $C_9H_{13}O_5$· that is formed by the initial OH attack and subsequent reactions. MCM v3.3.1 includes a BPR with the same structure but does not contain the subsequent reactions. The BPR of $C_9H_{13}O_5$· can be terminated via R5, forming a stabilized hydroxyl product of $C_9H_{14}O_4$, which is subject to a second OH attack and a following addition of O_2, resulting in a new peroxy radical of $C_9H_{15}O_7$·. There are no systematic investigations on the effect of a peroxide-bicyclic substitution on the 1,5 H-shift rate constant. However, our data indicate a hydrogen shift can occur on the 4-methyl group, based on which the structure of $C_9H_{15}O_9$· is proposed. The new BPR of $C_9H_{15}O_9$· is then terminated via R5, R6, and R7, forming stabilized products $C_9H_{14}O_8$, $C_9H_{16}O_8$, and $C_9H_{16}O_9$, respectively. This pathway is suggested by the observation of $C_9H_{12}D_2O_8$ in the 1,2,4-(4-methyl-D3)-TMB + OH experiment, though other pathways could result in products with the same formula.

An autoxidation reaction pathway that can explain the observation of $C_9H_{10}D_2O_7$ in the 1,2,4-(1-methyl-D3)-TMB + OH experiment is currently unavailable, although we speculate that a "peroxy-alkoxy-peroxy" conversion is likely involved during the formation of $C_9H_{12}O_7$ according to the number of oxygen atoms.

3.3 Characteristics of C18 HOMs

Products with 18 carbon atoms were observed in our experiments by Nitrate CI-APi-TOF, all containing 24-30 hydrogen atoms and 8 or more oxygen atoms ($C_{18}H_{24/26/28/30}O_{>8}$) (Figure 4). C18 products with 26 or 28 hydrogen atoms contributed the most of the signal intensities while those generated by 1,3,5-TMB were the most abundant. Recent studies revealed that long-neglected organic peroxide dimer (ROOR') formation reactions might be an important source of gas-phase dimer compounds, through which two peroxy radicals form accretion products consisting of the carbon backbone of both reactants (Berndt et al., 2018a, 2018b; Zhao et al., 2018).

$$RO_2 + R'O_2 \rightarrow ROOR' + O_2 \qquad (R8)$$

This reaction has been proved to be another important loss process for RO_2 radicals formed via autoxidation. On account of their extraordinarily low vapor pressure, HOM dimers contribute more significantly to the formation and growth of atmospheric new particles than HOM monomers.

Our C18 oxidation products have similar ion formulas to the dimer products in recent 1,3,5-TMB oxidation experiments (Molteni et al, 2018; Tsiligiannis et al., 2019). In our experiments, the formation of

$C_{18}H_{26}O_{8\text{-}15}$, $C_{18}H_{28}O_{9\text{-}15}$, and $C_{18}H_{30}O_{12\text{-}15}$ can be explained by reactions of two $C_9H_{13}O_x$·, one $C_9H_{13}O_x$·and one $C_9H_{15}O_x$·, and two $C_9H_{15}O_x$·respectively. $C_{18}H_{24}O_{8\text{-}13}$ with low signal intensities were detected by Nitrate CI-APi-TOF, hinting that H-abstraction reactions have occurred leading to a lower hydrogen atom in the product than in the precursor.

Figure 5 summarizes the relative contribution of C9 and C18 products formed from TMB oxidation as detected by Nitrate CI-APi-TOF. The charging efficiency for C9 and C18 products is assumed to be identical in Nitrate CI-APi-TOF (Ehn et al., 2014; Hyttinen et al., 2015). Hence, the measured relative abundances of the oxidation products, with corrections of the transmission function in the MS, can faithfully represent the product distribution in the experiments. In the Exp. #1-3, the dimers ($C_{18}H_{26}O_{8\text{-}15}$) formed from two $C_9H_{13}O_x$·along those ($C_{18}H_{28}O_{9\text{-}15}$) from one $C_9H_{13}O_x$·and one $C_9H_{15}O_x$·contributed the most intensity, whereas the most intensive C9 products ($C_9H_{14}O_{5\text{-}11}$) could be the alcohol or hydroperoxyl products of $C_9H_{13}O_x$·, or the carbonyl products of $C_9H_{15}O_x$· (Table S1). 1,2,3-TMB produced the most C9 products, 1,2,4-TMB the second, and 1,3,5-TMB the least. An opposite trend was observed for C18 products. Therefore, the reduction of C9 products was likely due to the dimer formation. Here, we define the C18 fraction as the ratio of the signal intensities of C18 products to the sum of those of C9 and C18 products in Nitrate CI-APi-TOF, and the C9 fraction in a similar way. According to our results, the dimer fraction was the highest for aromatics with meta-substituents and the least for aromatics with ortho-substituents, if the number and size of substituted groups are identical, while the monomer fraction had an opposite tendency. This can be explained by the stereoselectivity of accretion formation reactions. In the 1,3,5-TMB oxidation experiments (Exp. #2), where the highest C18 dimer fraction was observed, the mole fraction of the C18 dimers is likely determined by the competition of reactions R5, R6, R7, and R8, which can be mathematically expressed as

$$f_{C18} = \frac{0.5 \times k_{R8}[\mathrm{RO_2}]}{k_{R5,R6}[\mathrm{RO_2}] + k_{R7}[\mathrm{HO_2}] + 0.5 \times k_{R8}[\mathrm{RO_2}]} \qquad (\mathbf{1})$$

where $k_{R5,R6}$ stands for the reaction rates for R5 and R6, assumed to be around 8.8×10^{-13} cm^3 $molecule^{-1}$ s^{-1} by MCM, k_{R7} is the reaction rate for R7, set at a typical value of 2×10^{-11} cm^3 $molecule^{-1}$ s^{-1} (Berndt et al., 2018b; Bianchi et al., 2019), and k_{R8} is the reaction rate of R8 for BPRs generated by 1,3,5-TMB, which has recently been measured to be as fast as 10^{-10} cm^3 $molecule^{-1}$ s^{-1} (Berndt et al., 2018b).

Since the concentration of HO_2 in the OFR was not measured, we utilized a kinetic reaction model (PAM_chem_v8) to characterize the concentration profiles of oxidants in the OFR, which include OH, O_3, HO_2, and H_2O_2. A detailed description of this model is given in Section S1 of the supplement and the modelled profiles of oxidants and precursors are shown in Figure S4. According to the model, the steady-state concentration of HO_2 in the Exp. #2 was around 18 ppt (~ 4.5×10^8 molecules cm^{-3}). On the other hand, it is difficult to evaluate the effective concentration of the RO_2 radicals in the system, because RO_2 with low oxidation states will not form HOMs via reactions R5-R8. Therefore, we estimated the concentration of RO_2 in Eq. (1) to be close to that of BPRs in the OFR. According to MCM v3.3.1, the branching ratio for the peroxide-bicyclic pathway in the OH oxidation of 1,3,5-TMB is 79%, so that the concentration of BPRs was roughly estimated to be 58.5 ppb (~ 1.5×10^{12} molecules cm^{-3}, 79% of the reacted 1,3,5-TMB). Hence, the fraction of C18 dimer is estimated to be around 98%. Clearly, this

estimation itself comes with a large uncertainty, and the estimated fraction can only be regarded as an indication of explainable high yields of C18 dimers instead of a rigorous number.

In fact, under our experimental conditions, the C18 dimer fraction in the 1,3,5-TMB experiments was around 86.5%, which is much higher than the dimer fraction of 42.6%-56.5% re-calculated using the measured C9 and C18 signals by Tsiligiannis et al. (2019), 43.3%-52.4% modelled by Tsiligiannis et al. (2019), and 39% reported by Molteni et al. (2018). The lack of a m/z-transmission correction in the former two studies could partially explain the discrepancy (Molteni et al., 2018; Tsiligiannis et al., 2019). On the other hand, this observation could also be due to the much higher RO_2 concentrations in our experiments. The amount of reacted 1,3,5-TMB in our experiment is around 74.1 ppb (~ 1.8×10^{12} molecules cm^{-3}), whereas in the experiments of Tsiligiannis et al. (2019) and Molteni et al. (2018), the numbers are 26 ppb (~ 6.5×10^{11} molecules cm^{-3}) and 22.3 ppb (~5.6×10^{11} molecules cm^{-3}), respectively. Again, it should be reminded that this result was obtained under the condition of very high concentrations of precursors and thus the relative fractions of products could be different under the ambient conditions.

3.4 Influence of NO_x

To constrain the NO_x level in the OFR, the profiles of NO/NO_2 were modelled by PAM_chem_v8, as shown in Figure S5. The mathematically-averaged NO_x levels in the low NO_x experiment (Exp. #7) and higher NO_x experiment (Exp. #8) were 92 ppb (2.5 ppb NO + 89.5 ppb NO_2) and 295.3 ppb (2.9 ppb NO + 292.4 ppb NO_2), respectively. The NO_x/VOC in our experiments is comparable to ambient values in polluted areas. The NOx/(ΔVOC) was around 0.9 in the low NO_x experiment and 2.9 in the higher NO_x one.

Figure 6 describes the distribution of C9 products detected by Nitrate CI-APi-TOF in the absence of NO_x (Exp. #1), a low NO_x experiment (Exp. #7), and a higher NO_x experiment (Exp. #8), respectively. Once NO_x was added, the formation of C9 non-nitrogen products declined down to around 20% of those in Exp. #1. The production of C9 non-nitrogen products did not decrease much between low NO_x experiment and higher NO_x experiment, indicating a nonlinear effect of NO_x on the production of C9 non-nitrogen products. Dinitrates ($C_9H_xN_2O_y$) increased with the NO_x concentration, but C9 organonitrates (ONs, $C_9H_xNO_y$) slightly reduced in the higher NO_x experiment compared to that in the low one, which indicates a complex competition between $RO_2 + RO_2$ and $RO_2 + NO_x$.

The observation of C9 products containing 1-2 nitrogen atoms and C18 products with one nitrogen atom is similar to the results for 1,3,5-TMB oxidation experiments in the presence of NO_x reported by Tsiligiannis et al. (2019). NO_x can perturb the fate of peroxy radicals by the following reactions (Orlando and Tyndall, 2012; Rissanen, 2018):

$$RO_2 + NO \rightarrow RONO_2 \qquad (R9)$$

$$RO_2 + NO_2 \rightarrow RO + NO_2 \qquad (R10)$$

$$RO_2 + NO_2 \rightarrow RO_2NO_2 \qquad (R11)$$

Competing with the other RO_2 reactions, NO_x can dramatically reduce the formation of C9 non-nitrogen products.

Most organonitrates observed in our study were characterized with 13 hydrogen atoms, as detected by Nitrate CI-APi-TOF (Figure S2). All of them contained more than 6 oxygen atoms, with molecular formulas corresponding to bicyclic organonitrates formed from termination reactions of $C_9H_{13}O_x$· with NO or NO_2

(i.e., pathway R9 and R11, respectively). The dinitrates were dominated by species with 14 hydrogen atoms (Figure S3). As suggested by Tsiligiannis et al. (2019), an OH radical could attack a nitrated compound that is formed from NO_x termination of a peroxy radical, then an oxygen atom is added (similarly to the reactions from $C_9H_{14}O_7$ to $C_9H_{15}O_7$ in scheme 2), and then the newly formed peroxy radical that have already contained one nitrogen will be terminated by NO or NO_2 again. Therefore, most of the detected dinitrates were also formed from $C_9H_{13}O_x$·.

Figure 7a describes the relative intensities of C18 HOMs in Exp. #7, and Exp. #8 as detected by Nitrate CI-APi-TOF, in comparison with their relative intensities in Exp. #1. The relative intensities of most of the C18 HOMs decreased with the $NO_x/(\Delta VOC)$, while a few of the C18 HOMs including $C_{18}H_{24}O_{13}$, $C_{18}H_{26}O_{13}$, $C_{18}H_{26}O_{14}$, $C_{18}H_{28}O_{12}$ increased slightly in the higher NO_x experiment, potentially from a combined effect of NO_x and OH. The injection of NO_x can compete with the other RO_2 reactions, and thus it consumes peroxy radicals that would otherwise go through accretion reactions, which explains the decrease of most C18 HOMs. On the other hand, the introduction of NO_x can increase the oxidation capacity in the OFR, as it does in the ambient environment, leading to the slight enhancement for the few C18 HOMs. After the addition of NO_x, all of the C18 HOMs decreased by more than six times compared with those in no NO_x experiments, indicating that the dimers were more strongly influenced than monomers, which is in agreement with a previous study (Tsiligiannis et al., 2019).

The C18 ONs with 25 or 27 hydrogen atoms were detected in the NO_x experiments (Figure 7b). Other C18 products containing nitrogen atoms were not detected. The $C_{18}H_{25}NO_x$ might be formed from reactions between a $C_9H_{12}NO_x$· radical and a $C_9H_{13}O_x$· radical, or between a $C_9H_{14}NO_x$· and a $C_9H_{11}O_x$· radical, all of which existed in the system. The $C_{18}H_{27}NO_x$ is most likely to be formed from reactions between a $C_9H_{14}NO_x$· radical and a $C_9H_{13}O_x$· radical, which were the most abundant C9 radicals. All the C18 ONs decreased with the increase of $NO_x/(\Delta VOC)$, which is reasonable. Introduction of NO_x into the system triggered reactions between C9 peroxy radicals and NO_x, which consequently reduced the formation of accretion products like C18 ONs.

4 Conclusions

The identities and distribution of oxidation products formed from OH-initiated reactions of three TMBs were obtained with a suite of state-of-the-art chemical ionization mass spectrometers. Our recent study shows that the ring-retaining products are more oxygenated and quite a lot of carbon-carbon scission products are missed in the current model, indicating that the degradation products of aromatics are much more diverse than what is available in MCM (Mehra et al., 2020). Because of its important contribution to the nucleation and SOA formation in urban areas, the ring-retaining products of TMB deserve a more detailed characterization. Here we have built on that work by showing the formation pathways of ring-retaining highly oxygenated products and through identification of accretion products.

With the assistance of three 1,2,4-(methyl-D3)-TMB experiments we have demonstrated that the rapid formation of HOMs is attributable to the autoxidation pathway during the TMB oxidation. Several plausible autoxidation pathways for OH-initiated reactions of 1,2,4-TMB were proposed, emphasizing on the ring-retaining pathways of aromatics, especially the bicyclic-peroxide channel, which is followed by autoxidation that is not shown in the current models, such as MCM. Oxidation of aromatic VOCs was

shown in our study to produce HOM dimers, which might be underestimated or even completely ignored in previous studies which utilize techniques not capable of detecting dimers. The structural enhancement for accretion product formation via the RO_2 + $R'O_2$ reaction has been observed, of which the meta-substituents was shown to be strongest and ortho-substituents the weakest, though the detailed stereoselectivity for aromatics remains unclear now.

In the presence of NO_x whose reaction with RO_2· can compete with RO_2· + RO_2· or RO_2· + HO_2· reactions, ONs and dinitrates will be generated via reactions of NO_x with BPRs in 1,2,4-TMB oxidation system, and dimer products with one nitrogen will be formed via the subsequent reactions. This is consistent with recent ambient observations in the polluted environment, where ONs, dinitrates, and nitrogen-containing dimers presumably formed from BVOCs and alkylbenzenes were detected (Brean et al., 2019). The formation of ONs and dinitrates from TMB is not linearly dependent on the NO_x concentration, which excludes the possibility of extrapolating our laboratory results to ambient conditions. Nevertheless, the changes of HOM compositions in the presence of NO_x, especially the accretion products, could have an effect on NPF and SOA formation. Previous work has showed that the ring-retaining product formation at NO_x environment tends to be more important for TMB than other single substituted C9 aromatics, i.e., isopropylbenzene and propylbenzene, which emphasized the significance of TMB ring-retaining oxidation in the urban environment (Mehra et al., 2020). Further research is needed to acquire a quantitative understanding of the role of NO_x in HOM formation.

Clearly, these multifunctional gas phase products appear at different stages of the oxidation chain. These mass spectra can be used as ideal "fingerprints" of TMB oxidation in the ambient gas phase measurement to elucidate atmospheric oxidation conditions.

Data availability. Data related to this article will be available from a persistent repository and upon request from corresponding authors.

Supplement. The supplement related to this article is available online.

Author contributions. LW, and YW designed the experiments. YW, GY, XH, and YL carried out the instrument deployment and operation. AM, JK, and AL provided technical support. YW analyzed the data. YW, LW, and JK wrote the paper. All co-authors discussed the results and commented on the manuscript.

Competing interests. The authors declare that they have no conflict of interest.

Acknowledgments. This work was financially supported by the National Natural Science Foundation of China (91644213, 21925601) and the National Key R&D Program of China (2017YFC0209505). Lin Wang acknowledges the Newton Advanced Fellowship (NA140106).

References

Atkinson, R.: Kinetics and Mechanisms of the Gas-Phase Reactions of the Hydroxyl Radical with Organic Compounds under Atmospheric Conditions, Chem. Rev., 86(1), 69–201, doi:10.1021/cr00071a004, 1986.

Atkinson, R. and Arey, J.: Atmospheric Degradation of Volatile Organic Compounds, Chem. Rev., 103(12), 4605–4638, doi:10.1021/cr0206420, 2003.

Atkinson, R. and Carter, W. P. L.: Kinetics and Mechanisms of the Gas-Phase Reactions of Ozone with Organic Compounds under Atmospheric Conditions, Chem. Rev., 84(5), 437–470, doi:10.1021/cr00063a002, 1984.

Berndt, T., Richters, S., Jokinen, T., Hyttinen, N., Kurtén, T., Otkjær, R. V., Kjaergaard, H. G., Stratmann, F., Herrmann, H., Sipilä, M., Kulmala, M. and Ehn, M.: Hydroxyl radical-induced formation of highly oxidized organic compounds, Nat. Commun., 7(May), doi:10.1038/ncomms13677, 2016.

Berndt, T., Mentler, B., Scholz, W., Fischer, L., Herrmann, H., Kulmala, M. and Hansel, A.: Accretion Product Formation from Ozonolysis and OH Radical Reaction of α-Pinene: Mechanistic Insight and the Influence of Isoprene and Ethylene, Environ. Sci. Technol., 52(19), 11069–11077, doi:10.1021/acs.est.8b02210, 2018a.

Berndt, T., Scholz, W., Mentler, B., Fischer, L., Herrmann, H., Kulmala, M. and Hansel, A.: Accretion Product Formation from Self- and Cross-Reactions of RO 2 Radicals in the Atmosphere, Angew. Chemie Int. Ed., 57(14), 3820–3824, doi:10.1002/anie.201710989, 2018b.

Berndt, T., Scholz, W., Mentler, B., Fischer, L., Herrmann, H., Kulmala, M. and Hansel, A.: Accretion Product Formation from Self- and Cross-Reactions of RO2 Radicals in the Atmosphere, Angew. Chemie Int. Ed., 57(14), 3820–3824, doi:10.1002/anie.201710989, 2018c.

Bianchi, F., Kurtén, T., Riva, M., Mohr, C., Rissanen, M. P., Roldin, P., Berndt, T., Crounse, J. D., Wennberg, P. O., Mentel, T. F., Wildt, J., Junninen, H., Jokinen, T., Kulmala, M., Worsnop, D. R., Thornton, J. A., Donahue, N., Kjaergaard, H. G. and Ehn, M.: Highly Oxygenated Organic Molecules (HOM) from Gas-Phase Autoxidation Involving Peroxy Radicals: A Key Contributor to Atmospheric Aerosol, Chem. Rev., 119(6), 3472–3509, doi:10.1021/acs.chemrev.8b00395, 2019.

Bloss, C., Wagner, V., Jenkin, M. E., Volkamer, R., Bloss, W. J., Lee, J. D., Heard, D. E., Wirtz, K., Martin-Reviejo, M., Rea, G., Wenger, J. C. and Pilling, M. J.: Development of a detailed chemical mechanism (MCMv3.1) for the atmospheric oxidation of aromatic hydrocarbons, Atmos. Chem. Phys., 5(3), 641–664, doi:10.5194/acp-5-641-2005, 2005a.

Bloss, C., Wagner, V., Bonzanini, A., Jenkin, M. E., Wirtz, K., Martin-Reviejo, M. and Pilling, M. J.: Evaluation of detailed aromatic mechanisms (MCMv3 and MCMv3.1) against environmental chamber data., 2005b.

Brean, J., Harrison, R. M., Shi, Z., Beddows, D. C. S., Acton, W. J. F., Nicholas Hewitt, C., Squires, F. A. and Lee, J.: Observations of highly oxidized molecules and particle nucleation in the atmosphere of Beijing, Atmos. Chem. Phys., doi:10.5194/acp-19-14933-2019, 2019.

Calvert, J. G., Atkinson, R., Kerr, J. a., Madronich, S., Moortgat, G. K., Wallington, T. J. and Yarwood, G.: The Mechanisms of Atmospheric Oxidation of the Alkenes., 2000.

Crounse, J. D., Nielsen, L. B., Jørgensen, S., Kjaergaard, H. G. and Wennberg, P. O.: Autoxidation of organic compounds in the atmosphere, J. Phys. Chem. Lett., 4(20), 3513–3520, doi:10.1021/jz4019207, 2013.

D'Ambro, E. L., Lee, B. H., Liu, J., Shilling, J. E., Gaston, C. J., Lopez-Hilfiker, F. D., Schobesberger, S., Zaveri, R. A., Mohr, C., Lutz, A., Zhang, Z., Gold, A., Surratt, J. D., Rivera-Rios, J. C., Keutsch, F. N. and Thornton, J. A.: Molecular composition and volatility of isoprene photochemical oxidation secondary organic aerosol under low- and high-NOx conditions, Atmos. Chem. Phys., 17(1), 159–174, doi:10.5194/acp-17-159-2017, 2017.

Ehn, M., Thornton, J. A., Kleist, E., Sipilä, M., Junninen, H., Pullinen, I., Springer, M., Rubach, F., Tillmann, R., Lee, B., Lopez-Hilfiker, F., Andres, S., Acir, I. H., Rissanen, M., Jokinen, T., Schobesberger, S., Kangasluoma, J., Kontkanen, J., Nieminen, T., Kurtén, T., Nielsen, L. B., Jørgensen, S., Kjaergaard, H. G., Canagaratna, M., Maso, M. D., Berndt, T., Petäjä, T., Wahner, A., Kerminen, V. M., Kulmala, M., Worsnop, D. R., Wildt, J. and Mentel, T. F.: A large source of low-volatility secondary organic aerosol, Nature, 506(7489), 476–479, doi:10.1038/nature13032, 2014.

Eisele, F. L. and Tanner, D. J.: Measurement of the gas phase concentration of H2SO4 and methane sulfonic acid and estimates of H2SO4 production and loss in the atmosphere, J. Geophys. Res., doi:10.1029/93JD00031, 1993.

Garmash, O., Rissanen, M. P., Pullinen, I., Schmitt, S., Kausiala, O., Tillmann, R., Zhao, D., Percival, C., Bannan, T. J., Priestley, M., Hallquist, Å. M., Kleist, E., Kiendler-Scharr, A., Hallquist, M., Berndt, T., McFiggans, G., Wildt, J., Mentel, T. F. and Ehn, M.: Multi-generation OH oxidation as a source for highly oxygenated organic molecules from aromatics, Atmos. Chem. Phys., 20(1), 515–537, doi:10.5194/acp-20-515-2020, 2020.

Gueneron, M., Erickson, M. H., Vanderschelden, G. S. and Jobson, B. T.: PTR-MS fragmentation patterns of

gasoline hydrocarbons, Int. J. Mass Spectrom., 379, 97–109, doi:10.1016/j.ijms.2015.01.001, 2015.
Hallquist, M., Wenger, J. C., Baltensperger, U., Rudich, Y., Simpson, D., Claeys, M., Dommen, J., Donahue, N. M., George, C., Goldstein, A. H., Hamilton, J. F., Herrmann, H., Hoffmann, T., Iinuma, Y., Jang, M., Jenkin, M. E., Jimenez, J. L., Kiendler-Scharr, A., Maenhaut, W., McFiggans, G., Mentel, T. F., Monod, A., Prévôt, A. S. H., Seinfeld, J. H., Surratt, J. D., Szmigielski, R. and Wildt, J.: The formation, properties and impact of secondary organic aerosol: Current and emerging issues, Atmos. Chem. Phys., 9(14), 5155–5236, doi:10.5194/acp-9-5155-2009, 2009.
Heinritzi, M., Simon, M., Steiner, G., Wagner, A. C., Kürten, A., Hansel, A. and Curtius, J.: Characterization of the mass-dependent transmission efficiency of a CIMS, Atmos. Meas. Tech., 9(4), 1449–1460, doi:10.5194/amt-9-1449-2016, 2016.
Hyttinen, N., Kupiainen-Määttä, O., Rissanen, M. P., Muuronen, M., Ehn, M. and Kurtén, T.: Modeling the Charging of Highly Oxidized Cyclohexene Ozonolysis Products Using Nitrate-Based Chemical Ionization, J. Phys. Chem. A, 119(24), 6339–6345, doi:10.1021/acs.jpca.5b01818, 2015.
Isaacman-VanWertz, G., Massoli, P., O'Brien, R. E., Nowak, J. B., Canagaratna, M. R., Jayne, J. T., Worsnop, D. R., Su, L., Knopf, D. A., Misztal, P. K., Arata, C., Goldstein, A. H. and Kroll, J. H.: Using advanced mass spectrometry techniques to fully characterize atmospheric organic carbon: current capabilities and remaining gaps, Faraday Discuss., 200, 579–598, doi:10.1039/C7FD00021A, 2017.
Jenkin, M. E., Saunders, S. M. and Pilling, M. J.: The tropospheric degradation of volatile organic compounds: A protocol for mechanism development, Atmos. Environ., 31(1), 81–104, doi:10.1016/S1352-2310(96)00105-7, 1997.
Jenkin, M. E., Saunders, S. M., Wagner, V. and Pilling, M. J.: Protocol for the development of the Master Chemical Mechanism, MCM v3 (Part B): tropospheric degradation of aromatic volatile organic compounds, Atmos. Chem. Phys., 3(1), 181–193, doi:10.5194/acp-3-181-2003, 2003a.
Jenkin, M. E., Saunders, S. M., Wagner, V. and Pilling, M. J.: Protocol for the development of the Master Chemical Mechanism, MCM v3 (Part B): tropospheric degradation of aromatic volatile organic compounds, Atmos. Chem. Phys., 3(1), 181–193, doi:10.5194/acp-3-181-2003, 2003b.
Jokinen, T., Sipilä, M., Richters, S., Kerminen, V. M., Paasonen, P., Stratmann, F., Worsnop, D., Kulmala, M., Ehn, M., Herrmann, H. and Berndt, T.: Rapid autoxidation forms highly oxidized RO2 radicals in the atmosphere, Angew. Chemie - Int. Ed., 53(52), 14596–14600, doi:10.1002/anie.201408566, 2014.
Jokinen, T., Berndt, T., Makkonen, R., Kerminen, V. M., Junninen, H., Paasonen, P., Stratmann, F., Herrmann, H., Guenther, A. B., Worsnop, D. R., Kulmala, M., Ehn, M. and Sipilä, M.: Production of extremely low volatile organic compounds from biogenic emissions: Measured yields and atmospheric implications, Proc. Natl. Acad. Sci. U. S. A., 112(23), 7123–7128, doi:10.1073/pnas.1423977112, 2015.
Jørgensen, S., Knap, H. C., Otkjær, R. V., Jensen, A. M., Kjeldsen, M. L. H., Wennberg, P. O. and Kjaergaard, H. G.: Rapid Hydrogen Shift Scrambling in Hydroperoxy-Substituted Organic Peroxy Radicals, J. Phys. Chem. A, 120(2), 266–275, doi:10.1021/acs.jpca.5b06768, 2016.
Krechmer, J., Lopez-Hilfiker, F., Koss, A., Hutterli, M., Stoermer, C., Deming, B., Kimmel, J., Warneke, C., Holzinger, R., Jayne, J., Worsnop, D., Fuhrer, K., Gonin, M. and De Gouw, J.: Evaluation of a New Reagent-Ion Source and Focusing Ion− Molecule Reactor for Use in Proton-Transfer-Reaction Mass Spectrometry, Anal. Chem., 90, 12011–12018, doi:10.1021/acs.analchem.8b02641, 2018.
Krechmer, J. E., Coggon, M. M., Massoli, P., Nguyen, T. B., Crounse, J. D., Hu, W., Day, D. A., Tyndall, G. S., Henze, D. K., Rivera-Rios, J. C., Nowak, J. B., Kimmel, J. R., Mauldin, R. L., Stark, H., Jayne, J. T., Sipilä, M., Junninen, H., St. Clair, J. M., Zhang, X., Feiner, P. A., Zhang, L., Miller, D. O., Brune, W. H., Keutsch, F. N., Wennberg, P. O., Seinfeld, J. H., Worsnop, D. R., Jimenez, J. L. and Canagaratna, M. R.: Formation of Low Volatility Organic Compounds and Secondary Organic Aerosol from Isoprene Hydroxyhydroperoxide Low-NO Oxidation, Environ. Sci. Technol., 49(17), 10330–10339, doi:10.1021/acs.est.5b02031, 2015.
Kroll, J. H. and Seinfeld, J. H.: Chemistry of secondary organic aerosol: Formation and evolution of low-volatility organics in the atmosphere, Atmos. Environ., 42(16), 3593–3624, doi:10.1016/j.atmosenv.2008.01.003, 2008.
Kroll, J. H., Donahue, N. M., Jimenez, J. L., Kessler, S. H., Canagaratna, M. R., Wilson, K. R., Altieri, K. E., Mazzoleni, L. R., Wozniak, A. S., Bluhm, H., Mysak, E. R., Smith, J. D., Kolb, C. E. and Worsnop, D. R.: Carbon oxidation state as a metric for describing the chemistry of atmospheric organic aerosol, Nat. Chem., 3(2), 133–139, doi:10.1038/nchem.948, 2011.
Kwok, E. S. C. and Atkinson, R.: Estimation of hydroxyl radical reaction rate constants for gas-phase organic compounds using a structure-reactivity relationship: An update, Atmos. Environ., 29(14), 1685–1695, doi:10.1016/1352-2310(95)00069-B, 1995.
Lambe, A., Massoli, P., Zhang, X., Canagaratna, M., Nowak, J., Daube, C., Yan, C., Nie, W., Onasch, T., Jayne, J.,

631 Kolb, C., Davidovits, P., Worsnop, D. and Brune, W.: Controlled nitric oxide production via O(1D) + N2O
632 reactions for use in oxidation flow reactor studies, Atmos. Meas. Tech., 10(6), 2283–2298, doi:10.5194/amt-10-
633 2283-2017, 2017.
634 Lambe, A. T., Krechmer, J. E., Peng, Z., Casar, J. R., Carrasquillo, A. J., Raff, J. D., Jimenez, J. L. and Worsnop, D.
635 R.: HO x and NO x production in oxidation flow reactors via photolysis of isopropyl nitrite, isopropyl nitrite-d
636 7 , and 1,3-propyl dinitrite at λ = 254, 350, and 369 nm, Atmos. Meas. Tech., 12(1), 299–311, doi:10.5194/amt-
637 12-299-2019, 2019.
638 Lee, B. H., Lopez-Hilfiker, F. D., Mohr, C., Kurtén, T., Worsnop, D. R. and Thornton, J. A.: An iodide-adduct high-
639 resolution time-of-flight chemical-ionization mass spectrometer: Application to atmospheric inorganic and
640 organic compounds, Environ. Sci. Technol., 48(11), 6309–6317, doi:10.1021/es500362a, 2014.
641 Li, H., Riva, M., Rantala, P., Heikkinen, L., Daellenbach, K., Krechmer, J. E., Flaud, P.-M., Worsnop, D., Kulmala,
642 M., Villenave, E., Perraudin, E., Ehn, M. and Bianchi, F.: Terpenes and their oxidation products in the French
643 Landes forest: insight from Vocus PTR-TOF measurements, Atmos. Chem. Phys. Discuss., (September), 1–29,
644 doi:10.5194/acp-2019-741, 2019.
645 Li, R., Palm, B. B., Ortega, A. M., Hlywiak, J., Hu, W., Peng, Z., Day, D. A., Knote, C., Brune, W. H., De Gouw, J.
646 A. and Jimenez, J. L.: Modeling the radical chemistry in an oxidation flow reactor: Radical formation and
647 recycling, sensitivities, and the OH exposure estimation equation, J. Phys. Chem. A, 119(19), 4418–4432,
648 doi:10.1021/jp509534k, 2015.
649 Li, Y. and Wang, L.: The atmospheric oxidation mechanism of 1,2,4-trimethylbenzene initiated by OH radicals,
650 Phys. Chem. Chem. Phys., 16(33), 17908, doi:10.1039/C4CP02027H, 2014.
651 Lopez-Hilfiker, F. D., Mohr, C., Ehn, M., Rubach, F., Kleist, E., Wildt, J., Mentel, T. F., Lutz, A., Hallquist, M.,
652 Worsnop, D. and Thornton, J. A.: A novel method for online analysis of gas and particle composition:
653 Description and evaluation of a filter inlet for gases and AEROsols (FIGAERO), Atmos. Meas. Tech., 7, 983–
654 1001, doi:10.5194/amt-7-983-2014, 2014.
655 Lopez-Hilfiker, F. D., Iyer, S., Mohr, C., Lee, B. H., D'ambro, E. L., Kurtén, T. and Thornton, J. A.: Constraining
656 the sensitivity of iodide adduct chemical ionization mass spectrometry to multifunctional organic molecules
657 using the collision limit and thermodynamic stability of iodide ion adducts, Atmos. Meas. Tech., 9(4), 1505–
658 1512, doi:10.5194/amt-9-1505-2016, 2016.
659 Mentel, T. F., Springer, M., Ehn, M., Kleist, E., Pullinen, I., Kurtén, T., Rissanen, M., Wahner, A. and Wildt, J.:
660 Formation of highly oxidized multifunctional compounds: Autoxidation of peroxy radicals formed in the
661 ozonolysis of alkenes - Deduced from structure-product relationships, Atmos. Chem. Phys., 15(12), 6745–
662 6765, doi:10.5194/acp-15-6745-2015, 2015.
663 Molteni, U., Bianchi, F., Klein, F., Haddad, I. El, Frege, C., Rossi, M. J., Dommen, J. and Baltensperger, U.:
664 Formation of highly oxygenated organic molecules from aromatic compounds, Atmos. Chem. Phys, 18, 1909–
665 1921, doi:10.5194/acp-18-1909-2018, 2018a.
666 Molteni, U., Bianchi, F., Klein, F., El Haddad, I., Frege, C., Rossi, M. J., Dommen, J. and Baltensperger, U.:
667 Formation of highly oxygenated organic molecules from aromatic compounds, Atmos. Chem. Phys., 18(3),
668 1909–1921, doi:10.5194/acp-18-1909-2018, 2018b.
669 Nah, T., Sanchez, J., Boyd, C. M. and Ng, N. L.: Photochemical Aging of α-pinene and β-pinene Secondary Organic
670 Aerosol formed from Nitrate Radical Oxidation, Environ. Sci. Technol., 50(1), 222–231,
671 doi:10.1021/acs.est.5b04594, 2016.
672 Ng, N. L., Canagaratna, M. R., Zhang, Q., Jimenez, J. L., Tian, J., Ulbrich, I. M., Kroll, J. H., Docherty, K. S.,
673 Chhabra, P. S., Bahreini, R., Murphy, S. M., Seinfeld, J. H., Hildebrandt, L., Donahue, N. M., Decarlo, P. F.,
674 Lanz, V. A., Prévôt, A. S. H., Dinar, E., Rudich, Y. and Worsnop, D. R.: Organic aerosol components observed
675 in Northern Hemispheric datasets from Aerosol Mass Spectrometry, Atmos. Chem. Phys., 10(10), 4625–4641,
676 doi:10.5194/acp-10-4625-2010, 2010.
677 Orlando, J. J. and Tyndall, G. S.: Laboratory studies of organic peroxy radical chemistry: An overview with
678 emphasis on recent issues of atmospheric significance, Chem. Soc. Rev., 41(19), 6294–6317,
679 doi:10.1039/c2cs35166h, 2012.
680 Otkjær, R. V., Jakobsen, H. H., Tram, C. M. and Kjaergaard, H. G.: Calculated Hydrogen Shift Rate Constants in
681 Substituted Alkyl Peroxy Radicals, J. Phys. Chem. A, 122(43), 8665–8673, doi:10.1021/acs.jpca.8b06223,
682 2018.
683 Peng, Z., Day, D. A., Stark, H., Li, R., Lee-Taylor, J., Palm, B. B., Brune, W. H. and Jimenez, J. L.: HO x radical
684 chemistry in oxidation flow reactors with low-pressure mercury lamps systematically examined by modeling,
685 Atmos. Meas. Tech, 8, 4863–4890, doi:10.5194/amt-8-4863-2015, 2015.
686 Richters, S., Herrmann, H. and Berndt, T.: Different pathways of the formation of highly oxidized multifunctional

687 organic compounds (HOMs) from the gas-phase ozonolysis of β-caryophyllene, Atmos. Chem. Phys., 16(15),
688 9831–9845, doi:10.5194/acp-16-9831-2016, 2016.
689 Rissanen, M. P.: NO2 Suppression of Autoxidation-Inhibition of Gas-Phase Highly Oxidized Dimer Product
690 Formation, ACS Earth Sp. Chem., 2(11), 1211–1219, doi:10.1021/acsearthspacechem.8b00123, 2018.
691 Rissanen, M. P., Kurtén, T., Sipilä, M., Thornton, J. A., Kangasluoma, J., Sarnela, N., Junninen, H., Jørgensen, S.,
692 Schallhart, S., Kajos, M. K., Taipale, R., Springer, M., Mentel, T. F., Ruuskanen, T., Petäjä, T., Worsnop, D.
693 R., Kjaergaard, H. G. and Ehn, M.: The formation of highly oxidized multifunctional products in the ozonolysis
694 of cyclohexene, J. Am. Chem. Soc., 136(44), 15596–15606, doi:10.1021/ja507146s, 2014.
695 Rissanen, M. P., Kurtén, T., Sipilä, M., Thornton, J. A., Kausiala, O., Garmash, O., Kjaergaard, H. G., Petäjä, T.,
696 Worsnop, D. R., Ehn, M. and Kulmala, M.: Effects of chemical complexity on the autoxidation mechanisms of
697 endocyclic alkene ozonolysis products: From methylcyclohexenes toward understanding α-pinene, J. Phys.
698 Chem. A, 119(19), 4633–4650, doi:10.1021/jp510966g, 2015.
699 Riva, M., Rantala, P., Krechmer, J. E., Peräkylä, O., Zhang, Y., Heikkinen, L., Garmash, O., Yan, C., Kulmala, M.,
700 Worsnop, D. and Ehn, M.: Evaluating the performance of five different chemical ionization techniques for
701 detecting gaseous oxygenated organic species, Atmos. Meas. Tech, 12, 2403–2421, doi:10.5194/amt-12-2403-
702 2019, 2019.
703 Saunders, S. M., Jenkin, M. E., Derwent, R. G. and Pilling, M. J.: Protocol for the development of the Master
704 Chemical Mechanism, MCM v3 (Part A): Tropospheric degradation of non-aromatic volatile organic
705 compounds, Atmos. Chem. Phys., 3(1), 161–180, doi:10.5194/acp-3-161-2003, 2003.
706 Stolzenburg, D., Fischer, L., Vogel, A. L., Heinritzi, M., Schervish, M., Simon, M., Wagner, A. C., Dada, L.,
707 Ahonen, L. R., Amorim, A., Baccarini, A., Bauer, P. S., Baumgartner, B., Bergen, A., Bianchi, F.,
708 Breitenlechner, M., Brilke, S., Mazon, S. B., Chen, D., Dias, A., Draper, D. C., Duplissy, J., Haddad, I. El,
709 Finkenzeller, H., Frege, C., Fuchs, C., Garmash, O., Gordon, H., He, X., Helm, J., Hofbauer, V., Hoyle, C. R.,
710 Kim, C., Kirkby, J., Kontkanen, J., Kürten, A., Lampilahti, J., Lawler, M., Lehtipalo, K., Leiminger, M., Mai,
711 H., Mathot, S., Mentler, B., Molteni, U., Nie, W., Nieminen, T., Nowak, J. B., Ojdanic, A., Onnela, A.,
712 Passananti, M., Petäjä, T., Quéléver, L. L. J., Rissanen, M. P., Sarnela, N., Schallhart, S., Tauber, C., Tomé, A.,
713 Wagner, R., Wang, M., Weitz, L., Wimmer, D., Xiao, M., Yan, C., Ye, P., Zha, Q., Baltensperger, U., Curtius,
714 J., Dommen, J., Flagan, R. C., Kulmala, M., Smith, J. N., Worsnop, D. R., Hansel, A., Donahue, N. M. and
715 Winkler, P. M.: Rapid growth of organic aerosol nanoparticles over a wide tropospheric temperature range,
716 Proc. Natl. Acad. Sci. U. S. A., 115(37), 9122–9127, doi:10.1073/pnas.1807604115, 2018.
717 Teng, A. P., Crounse, J. D. and Wennberg, P. O.: Isoprene Peroxy Radical Dynamics, J. Am. Chem. Soc., 139(15),
718 5367–5377, doi:10.1021/jacs.6b12838, 2017.
719 Tröstl, J., Chuang, W. K., Gordon, H., Heinritzi, M., Yan, C., Molteni, U., Ahlm, L., Frege, C., Bianchi, F., Wagner,
720 R., Simon, M., Lehtipalo, K., Williamson, C., Craven, J. S., Duplissy, J., Adamov, A., Almeida, J.,
721 Bernhammer, A. K., Breitenlechner, M., Brilke, S., Dias, A., Ehrhart, S., Flagan, R. C., Franchin, A., Fuchs, C.,
722 Guida, R., Gysel, M., Hansel, A., Hoyle, C. R., Jokinen, T., Junninen, H., Kangasluoma, J., Keskinen, H., Kim,
723 J., Krapf, M., Kürten, A., Laaksonen, A., Lawler, M., Leiminger, M., Mathot, S., Möhler, O., Nieminen, T.,
724 Onnela, A., Petäjä, T., Piel, F. M., Miettinen, P., Rissanen, M. P., Rondo, L., Sarnela, N., Schobesberger, S.,
725 Sengupta, K., Sipilä, M., Smith, J. N., Steiner, G., Tomè, A., Virtanen, A., Wagner, A. C., Weingartner, E.,
726 Wimmer, D., Winkler, P. M., Ye, P., Carslaw, K. S., Curtius, J., Dommen, J., Kirkby, J., Kulmala, M.,
727 Riipinen, I., Worsnop, D. R., Donahue, N. M. and Baltensperger, U.: The role of low-volatility organic
728 compounds in initial particle growth in the atmosphere, Nature, 533(7604), 527–531, doi:10.1038/nature18271,
729 2016.
730 Tsiligiannis, E., Hammes, J., Salvador, C. M., Mentel, T. F. and Hallquist, M.: Effect of NOx on 1,3,5-
731 trimethylbenzene (TMB) oxidation product distribution and particle formation, Atmos. Chem. Phys., 19(23),
732 15073–15086, doi:10.5194/acp-19-15073-2019, 2019.
733 Wang, S., Wu, R., Berndt, T., Ehn, M. and Wang, L.: Formation of Highly Oxidized Radicals and Multifunctional
734 Products from the Atmospheric Oxidation of Alkylbenzenes, Environ. Sci. Technol., 51(15), 8442–8449,
735 doi:10.1021/acs.est.7b02374, 2017.
736 Wang, Y., Riva, M., Xie, H., Heikkinen, L., Schallhart, S., Zha, Q., Yan, C., He, X.-C., Peräkylä, O. and Ehn, M.:
737 Formation of highly oxygenated organic molecules from chlorine-atom-initiated oxidation of alpha-pinene,
738 Atmos. Chem. Phys., 20(8), 5145–5155, doi:10.5194/acp-20-5145-2020, 2020.
739 Yuan, B., Koss, A. R., Warneke, C., Coggon, M., Sekimoto, K. and De Gouw, J. A.: Proton-Transfer-Reaction Mass
740 Spectrometry: Applications in Atmospheric Sciences, Chem. Rev., 117(21), 13187–13229,
741 doi:10.1021/acs.chemrev.7b00325, 2017.
742 Zaytsev, A., Koss, A. R., Breitenlechner, M., Krechmer, J. E., Nihill, K. J., Lim, C. Y., Rowe, J. C., Cox, J. L.,

Moss, J., Roscioli, J. R., Canagaratna, M. R., Worsnop, D. R., Kroll, J. H. and Keutsch, F. N.: Mechanistic study of the formation of ring-retaining and ring-opening products from the oxidation of aromatic compounds under urban atmospheric conditions, Atmos. Chem. Phys., 19(23), 15117–15129, doi:10.5194/acp-19-15117-2019, 2019.

Zhang, Q., Jimenez, J. L., Canagaratna, M. R., Allan, J. D., Coe, H., Ulbrich, I., Alfarra, M. R., Takami, A., Middlebrook, A. M., Sun, Y. L., Dzepina, K., Dunlea, E., Docherty, K., DeCarlo, P. F., Salcedo, D., Onasch, T., Jayne, J. T., Miyoshi, T., Shimono, A., Hatakeyama, S., Takegawa, N., Kondo, Y., Schneider, J., Drewnick, F., Borrmann, S., Weimer, S., Demerjian, K., Williams, P., Bower, K., Bahreini, R., Cottrell, L., Griffin, R. J., Rautiainen, J., Sun, J. Y., Zhang, Y. M. and Worsnop, D. R.: Ubiquity and dominance of oxygenated species in organic aerosols in anthropogenically-influenced Northern Hemisphere midlatitudes, Geophys. Res. Lett., 34(13), 1–6, doi:10.1029/2007GL029979, 2007.

Zhao, Y., Thornton, J. A. and Pye, H. O. T.: Quantitative constraints on autoxidation and dimer formation from direct probing of monoterpene-derived peroxy radical chemistry, Proc. Natl. Acad. Sci., 115(48), 12142–12147, doi:10.1073/pnas.1812147115, 2018.

Ziemann, P. J. and Atkinson, R.: Kinetics, products, and mechanisms of secondary organic aerosol formation, Chem. Soc. Rev., 41(19), 6582–6605, doi:10.1039/c2cs35122f, 2012.

Table 1 Summary of experimental conditions.

#	Precursor	Experimental condition	Precursor concentration (ppb)	Consumption of precursor (%)	RH (%)	Total flow rate (slpm)	O_3 concentration (ppb)
1	1,2,4-TMB	OH	158	59.3	12.5	10	712
2	1,3,5-TMB	OH	118	62.8	13.6	10	845
3	1,2,3-TMB	OH	214	58.4	8.1	10	1426
4	1,2,4-(1-methyl-D3)-TMB	OH	155	62.0	11.6	10	1003
5	1,2,4-(2-methyl-D3)-TMB	OH	169	61.8	12.5	10	776
6	1,2,4-(4-methyl-D3)-TMB	OH	166	62.8	11.5	10	886
7	1,2,4-TMB	Low NO_x (2.5 ppb NO + 89.5 ppb NO_2) [a]	170	61.5	12.7	10.4	944
8	1,2,4-TMB	Higher NO_x (2.9 ppb NO + 292.4 ppb NO_2) [a]	145	69.7	9.3	10.4	3911

[a] Modelled mathematically-averaged NO/NO_2 concentrations in the OFR are shown here because of the malfunction of a NOx monitor. The model underestimates [NO] and [NO_2] by up to a factor of 2, according to separate experiments that are not presented.

Table 2. Oxidation products of 1,2,4-TMB in categories of carbonyl, hydroxyl, and hydroperoxyl according to their molecular mass, as well as the potential peroxy radicals. Numbers in the parenthesis denote the relative intensity detected by Nitrate CI-APi-TOF in the OH-initiated oxidation of 1,2,4-TMB when that of the largest HOM signal ($C_9H_{16}O_8$) is arbitrarily set to be 100%. The relative intensity has been corrected with the relative transmission efficiency of Nitrate CI-APi-TOF.

The potential peroxy radical *m*	Carbonyl *m*-17	Hydroxyl *m*-15	Hydroperoxyl *m*+1
$C_9H_{13}O_7$·	$C_9H_{12}O_6$ [a,b,c,d] (9.2 %)	$C_9H_{14}O_6$ [a,b,c,d] (20.3 %)	$C_9H_{14}O_7$ [b,c,d] (50.4 %)
$C_9H_{13}O_8$·	$C_9H_{12}O_7$ [b,c,d] (54.4 %)	$C_9H_{14}O_7$ [b,c,d] (50.4 %)	$C_9H_{14}O_8$ [c,d] (51.6 %)
$C_9H_{13}O_9$·	$C_9H_{12}O_8$ [d] (17.3 %)	$C_9H_{14}O_8$ [c,d] (51.6 %)	$C_9H_{14}O_9$ [d] (29.1 %)
$C_9H_{13}O_{10}$·	$C_9H_{12}O_9$ [d] (14.9 %)	$C_9H_{14}O_9$ [d] (29.1 %)	$C_9H_{14}O_{10}$ [d] (19.8 %)
$C_9H_{15}O_7$·	$C_9H_{14}O_6$ [a,b,c,d] (20.3 %)	$C_9H_{16}O_6$ [b,c,d] (2.3 %)	$C_9H_{16}O_7$ [b,c,d] (23.5 %)
$C_9H_{15}O_8$·	$C_9H_{14}O_7$ [b,c,d] (50.4 %)	$C_9H_{16}O_7$ [b,c,d] (23.5 %)	$C_9H_{16}O_8$ [c,d] (100 %)
$C_9H_{15}O_9$·	$C_9H_{14}O_8$ [c,d] (51.6 %)	$C_9H_{16}O_8$ [c,d] (100 %)	$C_9H_{16}O_9$ [d] (40.5 %)
$C_9H_{15}O_{10}$·	$C_9H_{14}O_9$ [d] (29.1 %)	$C_9H_{16}O_9$ [d] (40.5 %)	$C_9H_{16}O_{10}$ [d] (7.1 %)

[a] These compounds are listed in the MCM mechanism of 1,2,4-TMB where they are formed by multiple OH oxidation steps.

[b] These compounds were detected by Vocus PTR.

[c] These compounds were detected by Iodide CI-TOF in both gas and particle phase.

[d] These compounds were detected by Nitrate CI-APi-TOF.

Table 3. Partially deuterated C9 products observed by Vocus PTR and/or Nitrate CI-APi-TOF. “V” and “N” denote observation by Vocus PTR and Nitrate CI-APi-TOF, respectively, whereas “-" means that the product was not observed by any instrument.

	1,2,4-(1-methyl-D3)-TMB	1,2,4-(2-methyl-D3)-TMB	1,2,4-(4-methyl-D3)-TMB
$C_9H_{10}D_2O_6$	V, N	-	-
$C_9H_{10}D_2O_7$	V	-	-
$C_9H_{12}D_2O_8$	-	-	N

Scheme Captions

Scheme 1. A proposed autoxidation reaction scheme involving a bicyclic peroxy radical of $C_9H_{13}O_5$•.

Scheme 2. A proposed autoxidation reaction scheme involving a bicyclic peroxy radical of $C_9H_{13}O_5$•. Note that the reaction has been terminated with the formation of $C_9H_{14}O_4$ and re-initiated by a second OH attack.

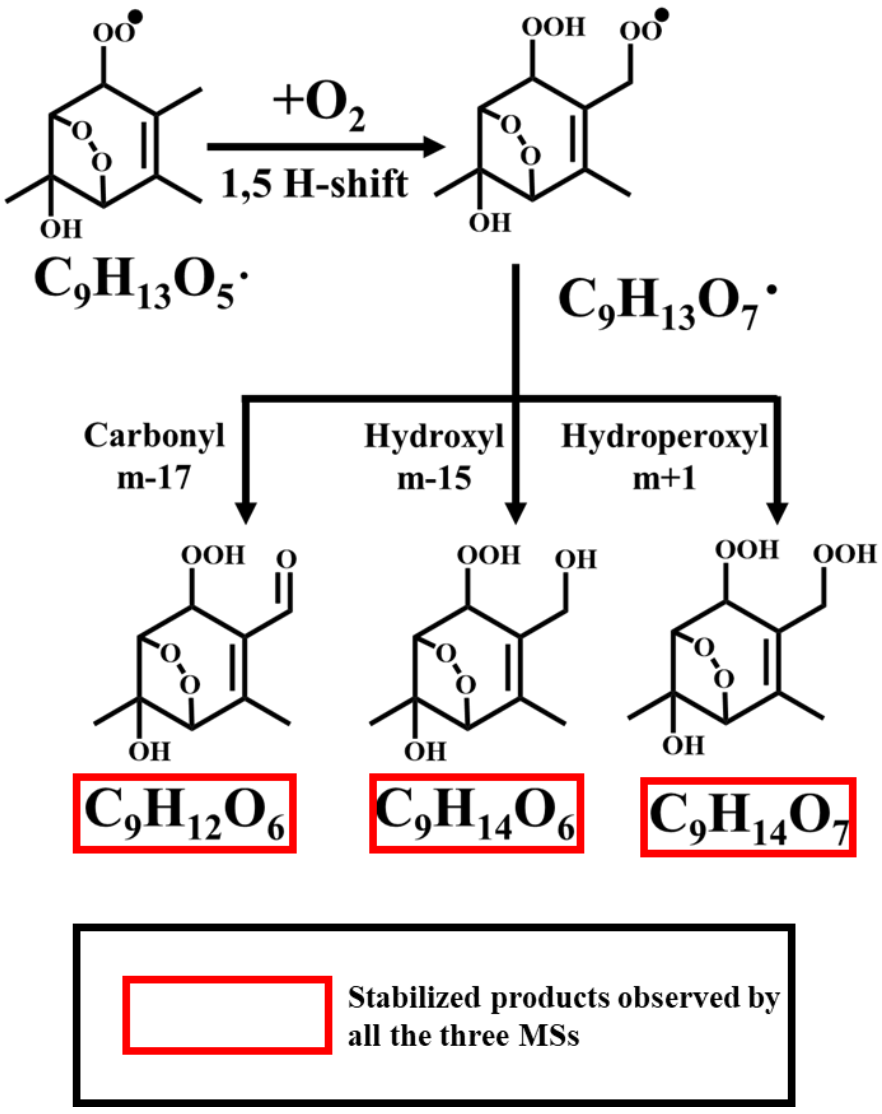
+O2
1,5 H-shift
C9H13O5·
C9H13O7·
Carbonyl
m-17
Hydroxyl
m-15
Hydroperoxyl
m+1
C9H12O6
C9H14O6
C9H14O7
Stabilized products observed by all the three MSs

Scheme 1

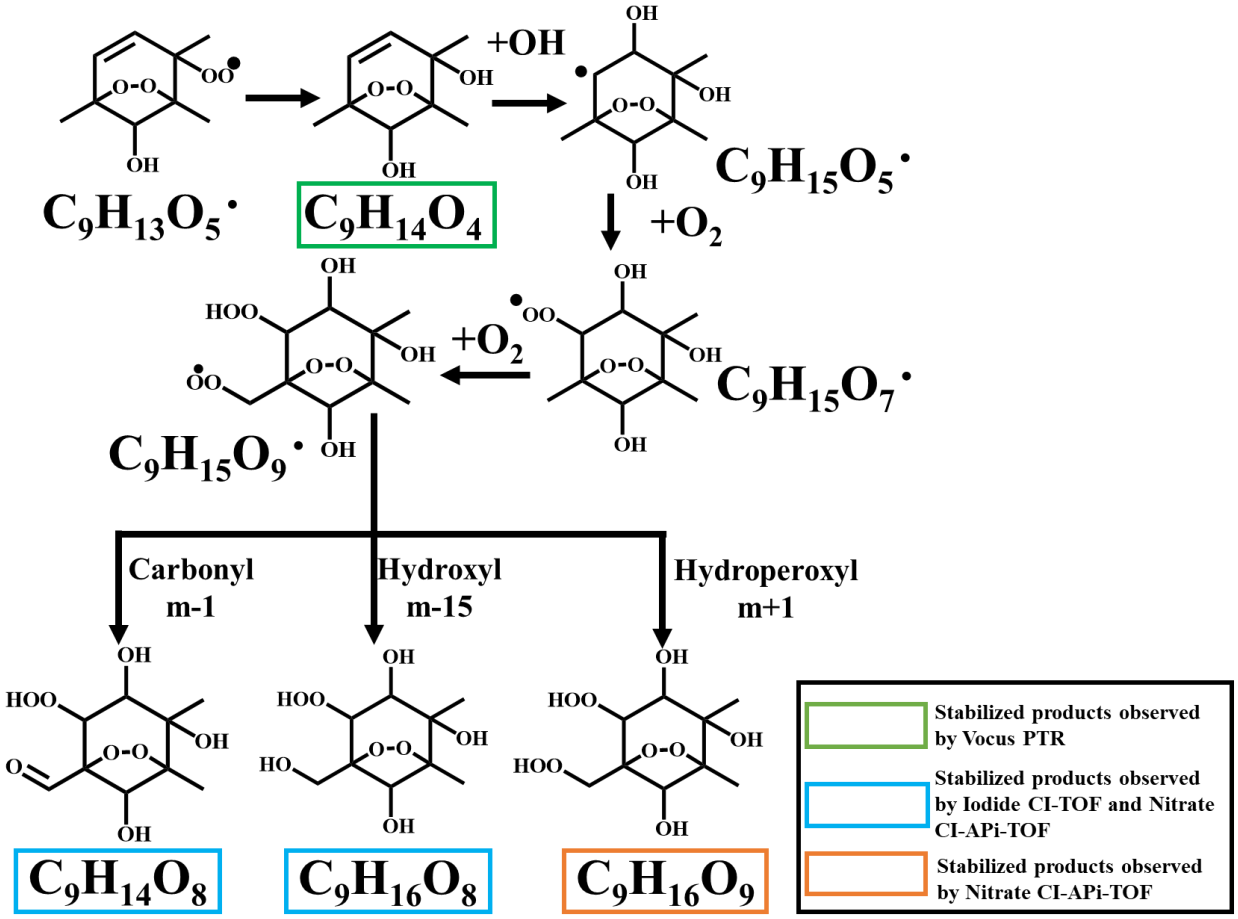
+OH
$C_9H_{13}O_5^{\bullet}$
$C_9H_{14}O_4$
$C_9H_{15}O_5^{\bullet}$
+O_2
+O_2
$C_9H_{15}O_7^{\bullet}$
$C_9H_{15}O_9^{\bullet}$
Carbonyl
m-1
Hydroxyl
m-15
Hydroperoxyl
m+1
$C_9H_{14}O_8$
$C_9H_{16}O_8$
$C_9H_{16}O_9$
Stabilized products observed by Vocus PTR
Stabilized products observed by Iodide CI-TOF and Nitrate CI-APi-TOF
Stabilized products observed by Nitrate CI-APi-TOF

Scheme 2

Figure Captions

Figure 1. Schematics of experimental setup.

Figure 2. Comparison of C7-C9 products observed in the OH-initiated oxidation of 1,2,4-TMB (Exp. #1 in Table 1) with those listed in the MCM mechanism (Bloss et al., 2005). Filled red, orange, and green circles denote observation by Nitrate CI-APi-TOF, Iodide CI-TOF, and Vocus PTR, respectively, whereas open blue circles represent MCM species. The radius of filled circles are proportional to the signals of the compounds in each instrument. The signal of the most abundant product for each instrument is arbitrarily set to be 100%, but note that the arbitrary signals are not comparable among instruments. Symbols have been offset horizontally to avoid overlap.

Figure 3. Distribution of C9 products formed from OH-initiated reactions of TMBs (Exp. #1- 3 in Table 1) by (a) Vocus PTR, (b) Iodide CI-TOF for the gas phase, (c) Iodide CI-TOF for particle phase, and (d) Nitrate CI-APi-TOF. The yield of the most abundant product for each instrument is arbitrarily set to be 100%, but note that the arbitrary yields are not comparable among instruments. Also note that signal of Vocus PTR was processed in a logarithmic way before calculating the arbitrary yield.

Figure 4. (a) Distribution of $C_{18}H_{24}O_{8\text{-}13}$ and $C_{18}H_{26}O_{8\text{-}15}$ products formed from TMB oxidation experiments (Exp. #1-3 in Table 1), as measured by Nitrate CI-APi-TOF; (b) Distribution of $C_{18}H_{28}O_{9\text{-}15}$ and $C_{18}H_{30}O_{12\text{-}15}$ formed from TMB oxidation experiments (Exp. #1-3 in Table 1), as measure by Nitrate CI-APi-TOF; and (c) The total signal of C18 products formed from TMB oxidation experiments (Exp. #1-3 in Table 1), as measure by Nitrate CI-APi-TOF.

Figure 5. Relative contribution of C9 and C18 products formed from TMB oxidation experiments, as measured by Nitrate CI-APi-TOF. The relative intensity has been corrected with the relative transmission efficiency.

Figure 6. Comparison of C9 products detected by Nitrate CI-APi-TOF with zero, one or two nitrogen atoms formed from 1,2,4-TMB oxidation with different NO_x settings.

Figure 7. (a) Comparison of C18 HOMs formed from 1,2,4-TMB oxidation with different NO_x settings; and (b) Distribution of C18 organonitrates fomed from 1,2,4-TMB oxidation.

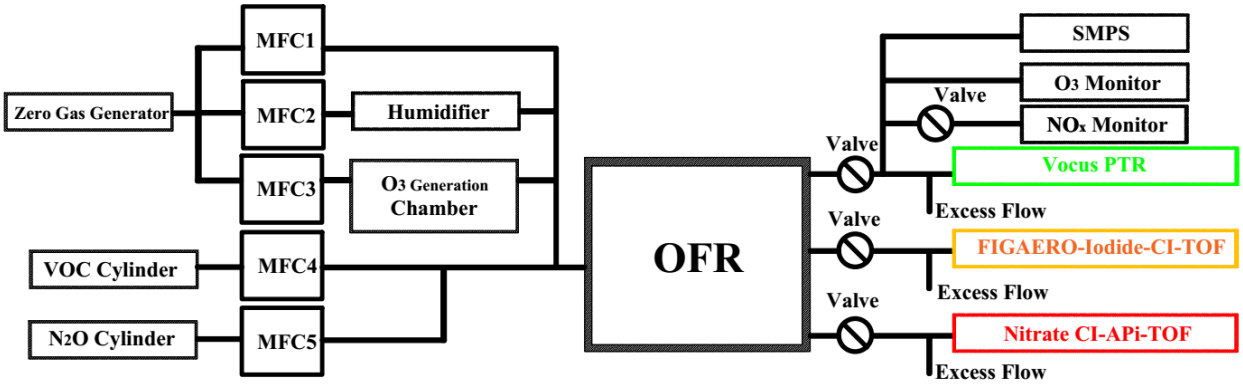
MFC1
Zero Gas Generator
MFC2
Humidifier
MFC3
O3 Generation Chamber
VOC Cylinder
MFC4
N2O Cylinder
MFC5
OFR
Valve
Valve
Valve
SMPS
O3 Monitor
NOx Monitor
Vocus PTR
Excess Flow
FIGAERO-Iodide-CI-TOF
Excess Flow
Nitrate CI-APi-TOF
Excess Flow

Figure 1

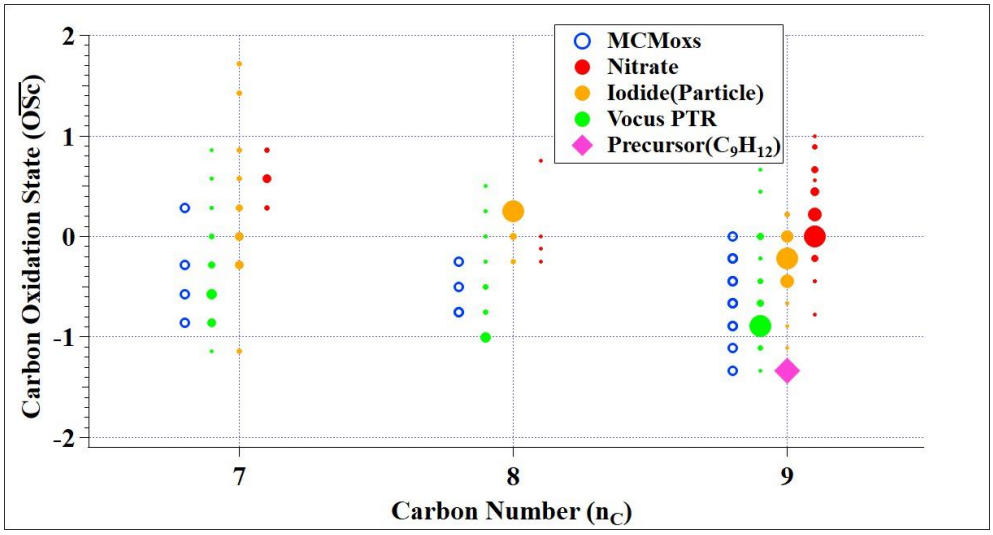
MCMoxs
Nitrate
Iodide(Particle)
Vocus PTR
Precursor(C_9H_{12})
Carbon Oxidation State ($\overline{OSc}$)
2
1
0
-1
-2
7
8
9
Carbon Number (n_C)

Figure 2

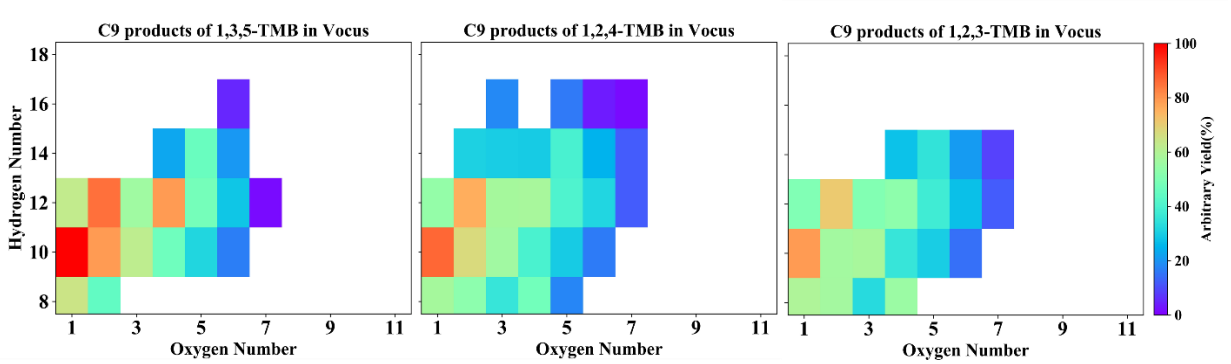

Figure 3a

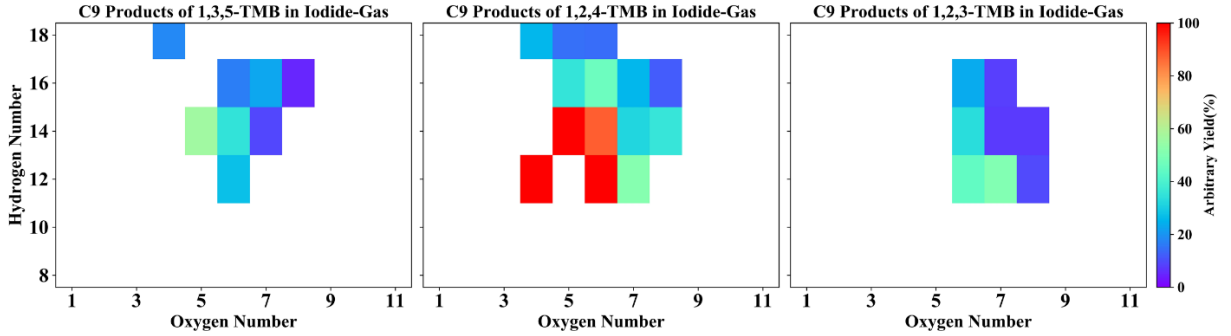

Figure 3b

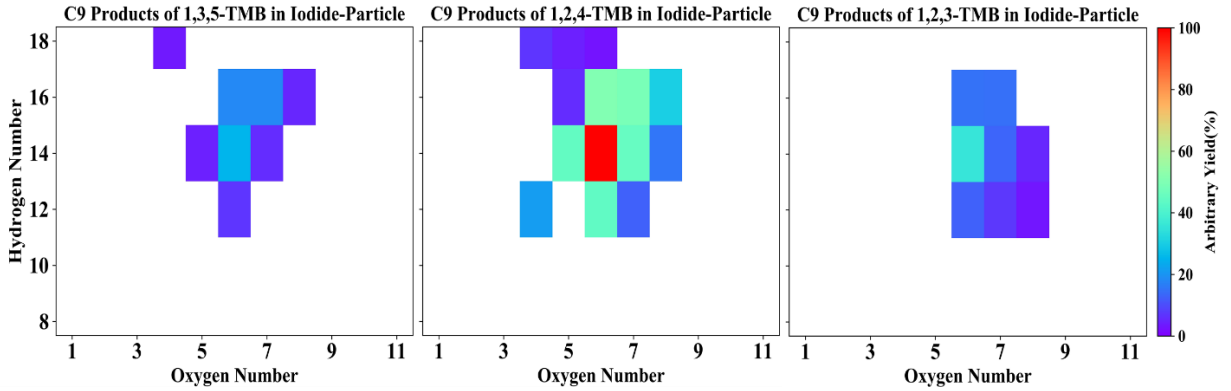

Figure 3c

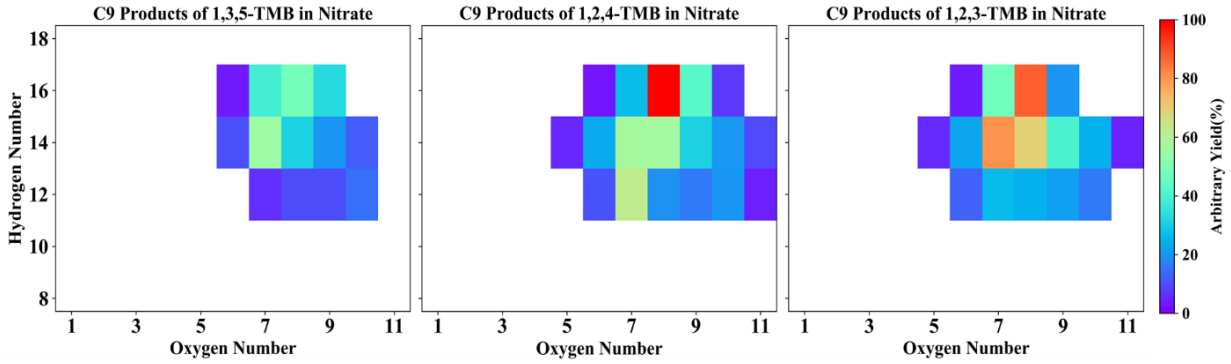

Figure 3d

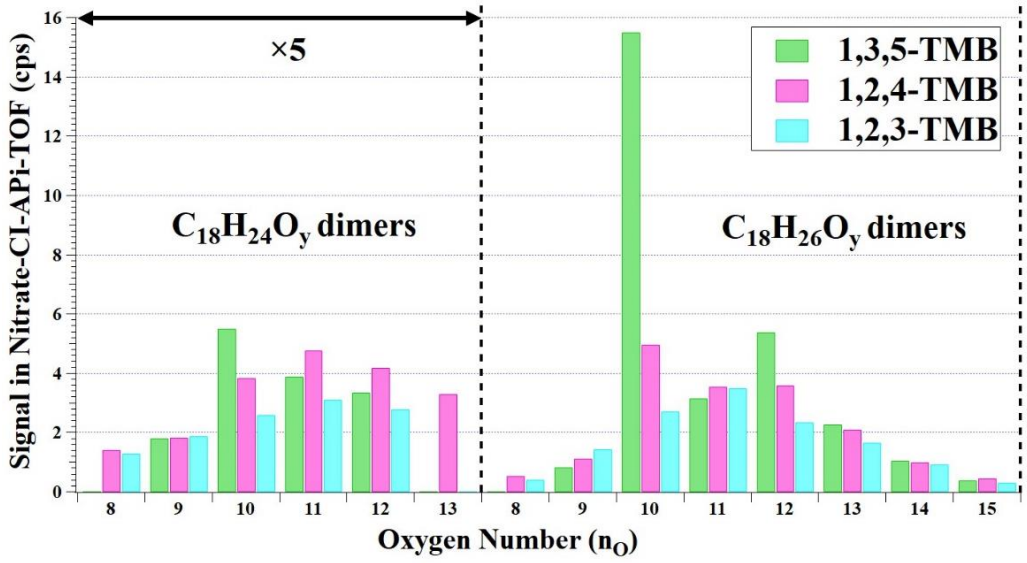

Figure 4a

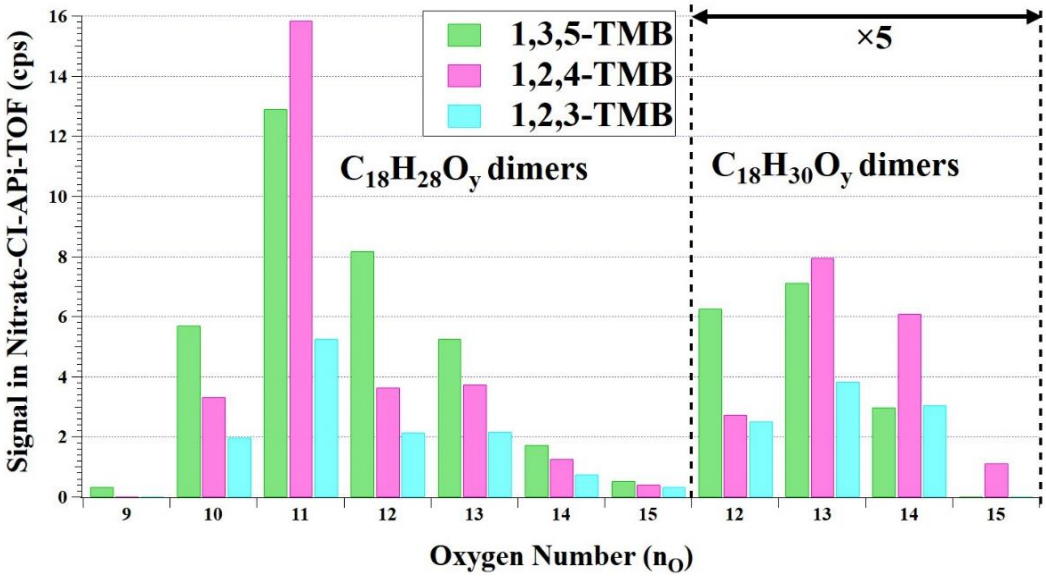

Figure 4b

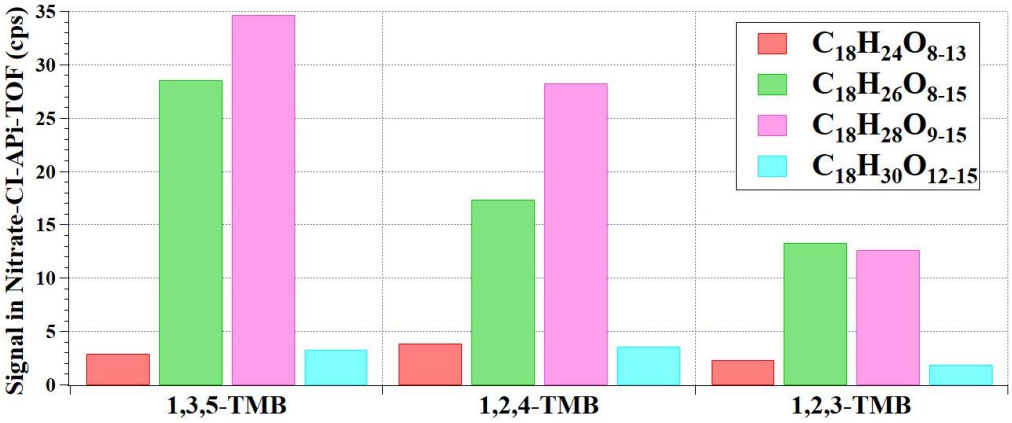
Signal in Nitrate-CI-APi-TOF (cps)
35
30
25
20
15
10
5
0
1,3,5-TMB
1,2,4-TMB
1,2,3-TMB
C18H24O8-13
C18H26O8-15
C18H28O9-15
C18H30O12-15

Figure 4c

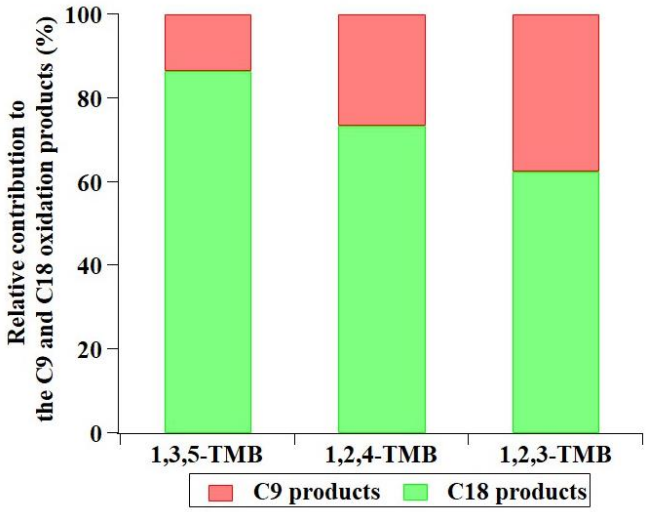
Relative contribution to
the C9 and C18 oxidation products (%)
100
80
60
40
20
0
1,3,5-TMB
1,2,4-TMB
1,2,3-TMB
C9 products
C18 products

Figure 5

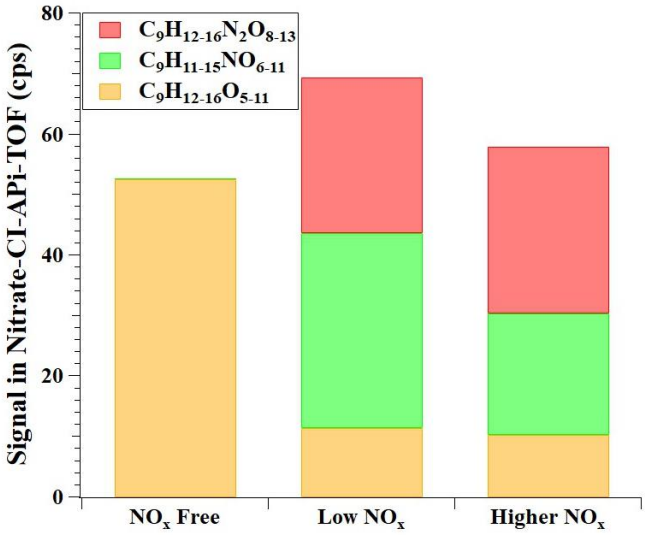
Signal in Nitrate-CI-APi-TOF (cps)
80
60
40
20
0
C9H12-16N2O8-13
C9H11-15NO6-11
C9H12-16O5-11
NOx Free
Low NOx
Higher NOx

Figure 6

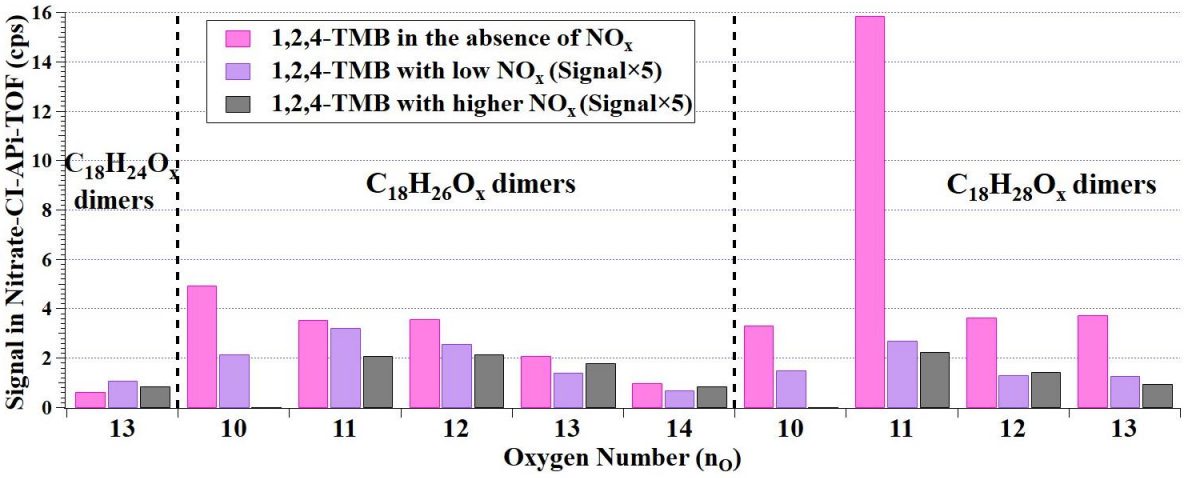

Figure 7a

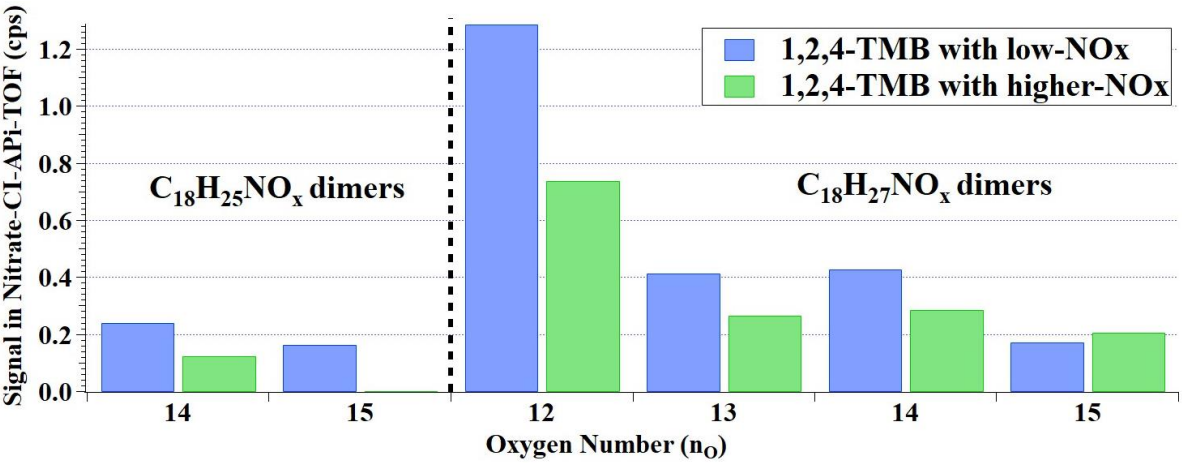

Figure 7b